INS-Rep.-769
Sept. 1989

INSTITUTE FOR NUCLEAR STUDY
UNIVERSITY OF TOKYO
Tanashi, Tokyo 188
Japan

Barium and xenon isotope yields in photopion reactions in cesium-133

K. SAKAMOTO, Y. HAMAJIMA, M. SOTO, Y. KUBOTA,
M. YOSHIDA, A, KUNUGISE and M. MASATANI

Department of Chemistry, Faculty of Science, Kanazawa University
Kanazawa 920, Japan

S. SHIBATA and M. IMAMURA

Institute for Nuclear Study, University of Tokyo
Tanashi, Tokyo 188, Japan

M. FURUKAWA

Department of Chemistry, Faculty of Science, Nagoya University
Nagoya 464, Japan

I. FUJIWARA

School of Economics, Otemon Gakuin University
Ibaragi, Osaka 567, Japan

INS-Rep.-769
Sept. 1989

Barium and xenon isotope yields in photopion reactions in cesium-133

K. SAKAMOTO, Y. HAMAJIMA, M. SOTO, Y. KUBOTA,
M. YOSHIDA, A, KUNUGISE and M. MASATANI

Department of Chemistry, Faculty of Science, Kanazawa University
Kanazawa 920, Japan

S. SHIBATA and M. IHAMURA

Institute for Nuclear Study, University of Tokyo
Tanashi, Tokyo 188, Japan

M. FURUKAWA

Department of Chemistry, Faculty of Science, Nagoya University
Nagoya 464, Japan

I. FUJIWARA

School of Economics, Otemon Gakuin University
Ibaragi, Osaka 567, Japan

Abstract The radiochemical yield measurements are reported of barium isotopes from $^{133}Cs(\gamma, \pi^- xn)^{133-x}Ba$ for x=0, 2, 4, 5, 6, 7 and 9 for bremsstrahlung maximum end-point energies (E_0)=30～1050 MeV and of ^{133}Xe from $^{133}Cs(\gamma, \pi^+)^{133m,g}Xe$ for E_0=300～1000 MeV. An emphasis was placed on Ba measurements around pion threshold and on runs for different target thickness to assess the interfering secondary particle-induced reactions. A clear evidence of the secondary reactions was found in a form of a shoulder of the yield curves in a range of $E_0 \lesssim Q_{\pi^-}$, the Q value of $^{133}Cs(\gamma, \pi^- xn)$ reaction, and used for the correction at $E_0 \gtrsim Q_{\pi^-}$ with aids of the reported measurements of the photoprotons from ^{12}C and other complex nuclei and the cross sections of (^{133}Cs+p) reactions.

The yields corrected for the secondaries, $\sigma_q(E_0)$, were unfolded into cross sections per photon of energy k, $\sigma(k)$. The characteristic features of $\sigma_q(E_0)$ and/or $\sigma(k)$ are then discussed in terms of E_0- and k-dependence and product mass (A_p=133-x), by comparing the present results with those currently obtained in our group. It was found that the present results of $\sigma(k)$ are grossly reproduced by a cascade-evaporation calculation based on the PICA code by Gabriel and Alsmiller, only if the calculated ones are shifted in photon energy by k=30 MeV higher and the cutoff energy for neutron is chosen to be 1 MeV.

I. INTRODUCTION

We report yield measurements for ^{133m}, ^{131m,g}, ^{129m,g}, ^{128}, ^{127}, ^{126}, ^{124}Ba from ^{133}Cs irradiated with bremsstrahlung beam with maximum end-point energies of E_0=30 to 1050 MeV in steps of 100 MeV and/or less. The preliminary results for ^{133m,g}Xe at E_0=300, 500, 700, 800, 900 and 1000 MeV are also included. These radionuclides are expected to be produced from ^{133}Cs(γ, π^-xn) and (γ, π^+) reactions. At energies above the pion threshold, the Δ isobar is expected to be produced by resonance interaction of an incoming photon with a single nucleon, N, inside the target nucleus. The isobar decays immediately (10^{-24} sec) into a stable nucleon and a pion, and both particles would usually develop a cascade-evaporation process in the same nucleus. During the process one of the two particles or both may have chance to escape from the nucleus. The probability of the escape may depend on location of Δ-formation and nuclear transparency for the associated particles. If the pion is emitted forward at small angles, the nucleus would be left with an energy insufficient for developing the cascade-evaporation process. Especially when the isobar production occurs at surface region of the target nucleus, the chance for escape would be high and the simple reactions such as (γ,n), (γ,p) and (γ, $\pi^{\pm}$) would be resulted. These simple reactions have received occasional attentions to gain valuable informations on photo-nuclear interaction and nuclear structure.[1,2] Additional emission of nucleons, especially neutrons, will also occur if sufficient energy is left after the primary process. Neutron

channels following pion emission have been studied far less extensively because of experimental complication of multi-particle coincidences, and of less attraction heretofore to nuclear physists. Otherwise the study has been limited to inclusive experiment of small degree.

Due to absence of high-energy monochromatic photon sources with sufficiently high intensity, a bremsstrahlung beam of continuous spectrum characterized approximately by 1/k, k being energies of constituent photons ranging from zero up to the end-point energy E_0, has been a unique tool in photonuclear reaction studies. Exceptions for this are the counter experiments where tagged photons and annihilation radiations have been used. With bremsstrahlung, the simple reactions are always accompanied by dominant reactions of single and multiple nucleon emissions, i.e. spallation, due to giant resonance and quasi-deuteron mechanisms caused by low-energy photons upto k=100 MeV and also due to cascade-evaporation process initiated by the Δ decay. Among these simple reactions, (γ, π^+) and $(\gamma, \pi^- xn)$ reactions of $x \geq 0$ are easily distinguished from other processes by use of radiochemical methods. Some measurements on (γ, π^+) on complex nuclei have been reported in the literature.[3-7] However, the study of the latter type of reactions has been reported only in very limited cases of $^{51}V(\gamma, \pi^-)^{51}Cr$(ref. 6), $^{51}V(\gamma, \pi^- 2n)^{49}Cr$(ref. 3,5,7-11) and $^{51}V(\gamma, \pi^- 3n)^{48}Cr$(ref. 11) and some others such as $^{197}Au(\gamma, \pi^- xn)^{197-x}Hg$ for x=0,2,4 and 5(ref. 12-14). A new clue to mechanism of photonuclear processes at intermediate energies is expected from a more thorough investigation of these photopion reactions.

A cursed problem in radiochemical methods is the presence of non-mesic interactions ; secondary protons and neutrons lead to the same products of $(\gamma, \pi^- xn)$ and (γ, π^+) reactions through (p,x'n) and (n,p) reactions, respectively. The emphasis in the present work was placed on runs below and above thresholds for pion production and on runs on target stacks of different thickness to assess the contribution of the interfering reactions. Successful correction of this contribution made it possible to characterize the new features of the cross section of the $(\gamma, \pi^- xn)$ reaction on complex nuclei. Comparison of the present results in a form of $\sigma(k)$, cross section per photon of monochromatic energy k, as a function of k was made with a cascade-evaporation calculation based on the Gabriel-Alsmiller's PICA code which has not been well tested with respect to $\sigma(k)$ since its publication as early as 1969,[15,16] and also with the total photoabsorption cross sections.

II. EXPERIMENTAL

Three to four disks of CsCl of about $0.35 \sim 0.5$ g/cm^2 of 1 cm in diameter were placed in a quartz tube as well as Al, Ni and/or Au monitors with thicknesses of 6.9(or 16.5), 13 and 100 mg/cm^2, respectively at both sides of each disk for beam monitor. Irradiations were carried out in a water-cooled target holder for $5 \sim 10$ min with un-collimated bremsstrahlung beam of maximum end-point energies of E_0=30 to 250 MeV from the 300 MeV Electron Linac of the Laboratory of Nuclear Science (LNS), Tohoku

University.[17] A series of irradiation for E_0=100 ~ 250 MeV was performed with electron beam passed through an energy compressing system,[18] with which the electron energy was confirmed to be ±1% at FWHM. Irradiation at E_0=305 MeV was performed in air at the Electro-technical Laboratory (ETL) for a similar target system to the one at LNS. For E_0=300 to 1050 MeV irradiations were performed in 50 MeV steps for 30 min to 8 hr in air with electron-free collimated bremsstrahlungs from the 1.3 GeV Electron Synchrotron of the Institute for Nuclear Study (INS), University of Tokyo. The target consisted of CsCl disks of 1 ~ 4 g/cm^2 in thickness and 2.5 cm × 2.5 cm in size stacked with Al beam monitors of 270 mg/cm^2. The beam intensity, which was 10^7 to 10^9 equivalent quanta/sec, was monitored with a Wilson-type thick chamber quantameter at INS, but the photon intensity used in the yield calculation for $E_0 \gtrsim 100$ MeV was obtained from the monitor reaction $^{27}Al(\gamma,2pn)^{24}Na$(ref. 19). The photon intensity for E_0=30 ~ 65 MeV was obtained from $^{197}Au(\gamma,n)^{196}Au$(ref. 20,21) in gold monitor foils. Average beam intensity from the LNS and ETL Linacs was $10^{12} \sim 10^{13}$ equivalent quanta/sec.

After irradiation, barium isotopes were separated with barium carrier and purified from aqueous solution of the CsCl target by a carbonate, nitrate and carbonate precipitation cycle and obtained finally as a $BaCO_3$ precipitate on a millipore Teflon filter. Xenon was adsorbed onto cooled charcoal after degassing from a melted CsCl disk and sealed in a glass ampoule. The gamma-ray measurements were performed with high purity Ge detectors of 1.6 to 1.7 keV resolution at 1332 keV coupled each

with a 4K pulse height analyser. The characteristic photopeaks were evaluated with an automatic peak-search program by Komura.[22] The peak assignment was based on energy and half-life, and the detector efficiency was determined with a calibrated ^{152}Eu and an uncalibrated ^{182}Ta sources of the same size as the sample. The relevant nuclear data were taken from the recent compilation[23,24] and shown in Table I. The chemical yields were determined by the weight of $BaCO_3$ and also by the comparison of photopeak counts of 496 keV of ^{131g}Ba, 81 keV of ^{133g}Xe, 233 keV of ^{133m}Xe and/or 148.9 keV of ^{123}Xe with those from a untreated CsCl disk from the same irradiation.

III. RESULTS AND DISCUSSIONS

The measured yields in unit of μb per equivalent quanta (μb/eq.q.) are given in Table II. The results obtained from multiplicate measurements are listed in separate entries. The associated errors are one standard deviation due to counting statistics. The yields of ^{133m}Xe and ^{133g}Xe were measured for E_0=300 (only for ^{133g}Xe), 500, 700, 800, 900 and 1000 MeV, but the quality of the data was poor because of low beam intensities of 10^7 eq.q. per sec and of low photopeak counts used in the chemical yield evaluation. The yield measurements of ^{133m}Ba, $^{131m,m+g}Ba$, $^{129m,m+g}Ba$, ^{128}Ba (and ^{128}Cs as the ^{128}Ba daughter), ^{127}Ba, ^{126}Ba and ^{124}Ba were more extensive, i.e. for E_0=30 to 1050 MeV in steps of 50 MeV or less. Only upper limits were obtained for the Ba yields at low E_0.

A. Yield curves

The variations of the Xe and Ba yields with E_0 are illustrated in Figs. 1(a) ~ (j). The insets in Fig. 1(a)~(i) show the details in the threshold region for pion production. Arrows on E_0 axis indicate Q values for production of radionuclides noted with their mass numbers from (n,p), (p,x'n) and (γ, $\pi^{\pm}$xn) reactions, i.e., Q_n^{133}, $Q_p^{134-x'}$ and $Q_{\pi^{\pm}}^{133-x}$, respectively. These show their relation to the threshold energies of the relevant reactions. Error bars are based on the values in Table II, and the data points without error bars indicate that the statistical uncertainty is within the size of the symbols. There are some discrepancies among the yield values for the same E_0 and for the neighboring E_0. The discrepancies over counting statistics arise mostly in our early measurements with insufficient beam intensities, and probably is caused by systematic errors such as large beam intensity fluctuation, etc. The multiple measurements resulted the yield data converging on a smooth solid curve shown in the respective figure. It is noted that the yields of Ba isotopes at E_0=30 to 250 MeV (±1%) measured at the LNS linac are smoothly connected to those for E_0=300 to 1050 MeV (±0.3%) measured at the INS synchrotron. The values at E_0=305 MeV measured at the ETL linac tend to be somewhat lower than the interpolated ones from the LNS and INS measurements. This discrepancy seems to be due to the difference in the converters, being W foil in the ETL irradiation and Pt foil in the LNS and INS irradiations.

Appreciable yields of Ba isotopes were observed at E_0 lower by several to a few tens of MeV than Q_{π^-}, and the reaction

thresholds are consistently higher than Q_p. After a steep rise from the threshold, the yields attain a plateau or a shoulder, which emerges around E_0=100 ~ 200 MeV, and again increase rapidly to attain the second plateau. The second rise starts from E_0 very close to Q_{π^-}. This feature is a clear evidence for the expected existence of two components ; one is ascribable to the secondary proton-induced reaction of $^{133}Cs(p,x'n)^{134-x'}Ba$ and the other is to $^{133}Cs(\gamma,\pi^-xn)^{133-x}Ba$ reaction. The former is superposed by the latter at $E_0 \geq Q_{\pi^-}$. The decomposition of the observed yields into the two components (the broken and dotted curves in Figs. 1(a) ~ (i)) is described in section C below.

The observed thresholds $(E_p)_{th}$ in E_0 of the secondary reactions, $^{133}Cs(p,x'n)^{134-x'}Ba$, are progressively higher for larger x' than Q_p. Recalling E_0 to be the bremsstrahlung maximum end-point energy and $(E_p)_{th}$ to be the observed threshold energies in E_0 of the secondary-proton induced reactions through the $(\gamma,xnyp)$ reactions in the target by the same bremsstrahlung, the relationship of $(E_p)_{th}$ and Q_p reflects the energy spectra of protons produced in the CsCl target. Actually $(E_p)_{th}$ was found to vary linearly with Q_p.

The variation of the yields after the second steep rise is not appreciable within experimental uncertainty for all radionuclides observed, and suggests that photons responsible for production of these nuclides are mostly of energies lower than 400 MeV but higher than 140 MeV (pion threshold), in accordance with the reported yield curves for $(\gamma,\pi^{\pm})$ reactions on complex nuclei[3-7] and for (γ,π^-xn) reactions on ^{51}V(refs. 3,5,7-11).

See section C for further characteristic features of the (γ , π^- xn) yields.

B. Depth profiles

Additional measurements of the Ba yields were performed on a thick target stacked with many disks of CsCl and foils of Al and Ni for E_0=500, 700 and 800 MeV to assess the secondary reactions. The results of the depth profiles were essentially the same for the three E_0. The 800 MeV result is shown in Fig. 2, where radioactivities per unit weight of the targets are normalized to those of the front target. The numbers in parentheses are the Q values in MeV for production of the isotopes of Ni, Co, V and Mn from ^{58}Ni, ^{24}Na from ^{27}Al, and Ba from ^{133}Cs. The two values for ^{131}Ba and ^{126}Ba are shown ; one on the left is for ^{133}Cs(p,x'n) and the other on the right is for ^{133}Cs(γ , π^-xn) reaction. The yields of the Ba isotopes, together with ^{48}V, ^{54}Mn and ^{24}Na, all from the reactions with Q values larger than about 25 MeV do not increase with increase of target depth, contrary to the expected trend for secondary particle effects. The degree of the decrease with depth is qualitatively in the order of increase of particle multiplicity or of the Q value, if the Ba production is assumed to be from the (γ , π^-xn) reaction. The yields of ^{57}Ni expected from ^{58}Ni(γ ,n) and (n,2n), the Q value of which is 12 MeV, increase rapidly with depth, while those of ^{56}Ni from ^{58}Ni(γ ,2n) and (n,3n) of Q=23 MeV, and ^{58}Co from ^{60}Ni(γ ,pn) and ^{58}Ni(n,p) reactions of Q=20 MeV, increase slightly with depth. Productions of ^{57}Ni and ^{56}Ni from ^{60}Ni (26.10%) and the other heavier Ni isotopes would be less

important than those from ^{58}Ni (67.76%). The decrease and/or the increase of the yields may be explained as caused by absorption of the bremsstrahlung mainly due to e^+e^- pair creation and a build up of secondary low-energy photons and particles in the target stack, resulting at depths in suppression by absorption of photons of energies above pion threshold and in enhancement of, in addition to absorption of, photons responsible for the reactions of smaller Q values. The difference in the depth profiles of the Ba yields and of the ^{24}Na yields suggests that the Al monitor reaction employed for the Ba yield determination is inadequate for a thick target located deep in a target stack. The yields presented in Table II and Fig. 1 are those obtained from a front target disk of less than 4 g/cm^2. It is now concluded that the secondary contribution can not be estimated from the depth profile.

C. Correction for secondary reactions

The contribution of the secondary reaction to the observed Ba yields was then estimated from the shoulder at $E_0 < Q_\pi$ in the yield curve. The estimation at $E_0 > Q_\pi$ was performed on the basis of the reported photoproton spectra at 40° (ref. 25) and 72° (ref. 26) from ^{12}C and some other complex nuclei[27] and the measured and calculated excitation functions for ^{133}Cs(p,x'n)$^{134-x'}$Ba (ref. 28). The calculation of the proton excitation functions was aided by the ALICE code.[29,30] For $E_p \geq 90$ MeV, the proton cross sections were assumed to decrease exponentially, i.e. $\sigma(90\ \text{MeV}) \cdot \exp(-aE_p)$, a being an adjustable parameter obtained by fitting to the ALICE results at $E_p \leq 90$ MeV. The

photoproton spectra at high energies were assumed to be isotropic for a heavier target under study and originated in quasi-deuteron mechanism with the Levinger constant, L=5 ~ 13(Ref.23). The photoproton spectra at low energies were not available, and assumed to be of a Maxwellian shape. The absolute values were estimated by fitting the calculated ^{131}Ba yields and ^{51,49}Cr yields from ^{51}V(p,x'n) reaction[7] to the corresponding ones observed below Q_{π^-}, assuming that the latters are entirely from the secondaries. A good fit to the yields of ^{131}Ba was obtained, and is shown by the broken curve as noted as $(^{131}Ba)_p$ in Fig. 1(c). However, the $(Ba)_p$ yields for the other Ba nuclides calculated with the same proton spectrum were adjusted by multiplying them by factors of 1.8 for ^{129}Ba, 1.4 for ^{128}Ba, 2.0 for ^{127}Ba and 2.0 for ^{126}Ba, keeping the shapes as calculated to obtain good fits to the observed shoulders. For the metastable isomer yields, the ALICE results for the formation cross sections of the ground-state isomers were tentatively used and good fits to the observed yields of $(^{133m,131m,129m}Ba)_p$ at $E_0 \lesssim Q_{\pi^-}$ were obtained by multiplying the calculated results by 0.12, 0.49 and 1.14, respectively. The different adjustments of the calculated $(^{134-x'}Ba)_p$ required in the fitting suggest that there still remain ambiguities mostly in the photoproton spectra used in the calculation. The results of the fitting are shown by the broken curves, and the subtraction of the $(^{134-x'}Ba)_p$ from the observed yields results in the net yields which are shown by the dotted curves noted as $(^{133-x}Ba)_{\pi^-}$ in Fig. 1(a)~(i). The relative contributions of the secondaries, $(^{134-x'}Ba)_p$, to the

observed yields, $(^{133-x}Ba)_{obs}$, at $E_0 \geq 500$ MeV decrease with increase of x'. At E_0=1000 MeV they are about 15% for $^{133m}Ba(x'=1)$, 14% for $^{131m,m+g}Ba(x'=3)$, 10% for $^{129m,m+g}Ba(x'=5)$, 7% for $^{128}Ba(x'=6)$, 6% for $^{127}Ba(x'=7)$ and 5% for $^{126}Ba(x'=8)$. The amount of ^{124}Ba from $^{133}Cs(p,9n)$ was estimated from this trend, but $(^{133}Xe)_n$ from $^{133}Cs(n,p)$ was unable to obtain due to lack of $(^{133}Xe)_{obs}$ at $E_0 < Q_{\pi^+}$. The yields of ^{133}Xe and ^{133m}Xe are regarded to be the upper limits of $^{133}Cs(\gamma, \pi^+)$ yields.

D. Mass yield curves

It is interesting to see the mass yield features, which are shown in Fig. 3. Here the yields of $^{133-x}Ba$ from $^{133}Cs(\gamma, \pi^- xn)$ reactions are plotted against the number (x) of neutrons emitted at some selected E_0, comparing with those of $^{51}V(\gamma, \pi^- xn)^{51-x}Cr$ as reported in ref. 7. For E_0=400 to 1050 MeV, the averaged values are taken. One standard deviation of the mean is shown by error bars. Also plotted by elongated diamonds are the averages of the measured yields of ^{133m}Xe and $^{133(m+g)}Xe$, not corrected for the secondaries. The open symbols connected with dotted curves are for the yields of the high-spin metastable isomers (m) and the closed ones connected with solid curves are for those plus the low-spin ground state isomers (g). The mass yield patterns for m and (m+g) look quite similar at each E_0. The shapes of the mass yield curves are quite different for the two targets. The maximum yields for $^{133-x}Ba$ from ^{133}Cs seem to locate at $x \approx 3$ for E_0=250 to 1050 MeV and the excitation energies left in the target nucleus after π^- emission are high enough to evaporate 7 to 9 neutrons with appreciable probability. It is

noted for ^{133}Cs that these multiple neutron emissions are far more probable than the (γ, π^-) channel which has no prominent E_0-dependence. The mass yield patterns[7] for a lighter target, ^{51}V for x=0, 2 and 3, show a systematic variation quite different from those of ^{133}Cs ; the maximum yields occur at $x \approx 0$ in $^{51}(\gamma, \pi^- xn)$ reaction even for E_0=400 ~ 1000 MeV. For both targets, the (γ, π^+) channel is a factor of 5 lower than the (γ, π^-) reaction at all E_0 studied.

The excitation energies left after pion emission are approximated by the sum of neutron separation energies (7 MeV/neutron on average) of the product nuclides. Averaged neutron multiplicities $\bar{x}$ of 2 and 7 for the Cr and Ba yields are 14 and 50 MeV, respectively. Their ratio of 3.5 is consistent with the ratio of the target neutrons, $N_t(^{133}Cs)/N_t(^{51}V)$=3.4. This suggests that all the neutrons in the target nucleus are equally involved in Δ formation ; $n + \gamma \longrightarrow \Delta \longrightarrow \pi^- + p$.

E. Unfolding of yield curves

The Ba yields, $\sigma_q(E_0)$, corrected for the secondary reactions were unfolded into cross sections per photon of energy k, $\sigma(k)$, after the method of Tesch[31] with an aid of LOUHI-82 code.[32] In the unfolding calculation, the Schiff spectrum[33] was used for approximation of bremsstrahlung production cross section. The results for $\sigma(k)$ are illustrated in Fig. 4; (a) is for the isomer pairs and (b) is for the ground states respectively. It is shown that all the excitation curves are of similar resonant shape with FWHM of (70 ±15) MeV and with peak

energies of 210 to 340 MeV for x=0 to 9 (Fig. 5). FWHM increases slightly, within the range of (70 ± 15) MeV, with increase of x. Unmeasured cross sections for x=1 (^{132}Ba), x=3 (^{130}Ba) and x=8 (^{125}Ba) were estimated by interpolation of peak energies shown in Fig. 5 and peak cross sections which are quite similar in shape to the mass yield curve of 400-1000 MeV in Fig. 3, FWHM (=70 MeV), FWQM (=45 ± 10 MeV), FWTM (=180 ± 25 MeV) and a linear relationship of thresholds and Q values, of the unfolded ones, and shown by broken curves in Fig. 4.

As mentioned earlier, a Monte Carlo intranuclear cascade-evaporation analysis code (PICA) developed by Gabriel and Alsmiller, Jr.[15,16] has not been well tested for $\sigma(k)$ for production of residual nuclei from (3,3)-resonance. Our recent work[7] showed that this calculation code could reproduce our $\sigma(k)$ of $^{51}V(\gamma, \pi^- xn)^{51-x}Cr$ for x=0, 1, 2 and 3 and $^{51}V(\gamma, \pi^+)^{51}Ti$ within a factor of two, provided that all the calculated results were shifted higher in k axis by 30 MeV for ^{51-x}Cr and by 60 MeV for ^{51}Ti. The same calculation was extended in the present work to $^{133}Cs(\gamma, \pi^- xn)^{133-x}Ba$ reaction of much higher neutron multiplicity (x) upto 9 for k=150 to 400 MeV. The same parameter values were chosen as those of the original authors except for some alternative sets of cutoff energies for emitted particles. The results of the calculation with the cutoff energies of 5 MeV for charged particles and 1 MeV for neutron are plotted in Fig. 6(a) for the even mass products and in Fig. 6(b) for the odd mass products, as connected by the dotted curves to guide the eye. Events for the ^{124}Ba production were too small to appear in the particle histories of $(0.2 \sim 1) \times 10^6$. Error

bars associated with the calculated points are of statistical ones. The solid curves are the same as in Fig. 4. Note that the k-axis is different for the two, i.e. all the peak locations of the calculated curves can be fitted very well to the experimental ones by shifting the former by 30 MeV higher, as was in the case of $^{51}V(\gamma, \pi^- xn)^{51-x}Cr$. Reproduction of the peak cross sections of the even mass products are excellent, but for the odd mass products the calculated peak cross sections are lower by 100% for ^{133}Ba, 15% for ^{131}Ba and 7% or less for ^{129}Ba, but higher by 50% for ^{127}Ba than the corresponding experimental ones. These features of the peak cross sections are caused by a strong even-odd effect in the calculation as depicted in Fig. 7. The even-odd feature of the PICA results for $^{51}V(\gamma, \pi^- xn)^{51-x}Cr$ was also evident but opposite : the odd mass yields were reproduced much better than the even ones. Different sets of cutoff energies for charged particles and neutron of 10 and 0 MeV, 10 and 5 MeV, and 5 and 0 MeV, respectively, yielded still higher peak values at $x>3$ ($^{130}Ba \sim ^{127}Ba$), while those at $x \lesssim 2$ ($^{133}Ba \sim ^{131}Ba$) remained the same. It is noted that in the calculation for $\sigma(k)$ for $^{51}V(\gamma, \pi^- xn)$ reaction no prominent difference was obtained from different sets of the cutoff energies. The calculation for the high energy part of the tail gave $\sigma(k)$ somewhat higher than the experimental one on the whole. However, it may be concluded that the PICA code reproduces well the gross feature of $\sigma(k)$ at Δ-resonance if the energy shift of 30 MeV for $(\gamma, \pi^- xn)$ reaction (and 60 MeV for (γ, π^+) reaction) as mentioned above are accounted.

In Fig. 8, the sum of $\sigma(k)$ for $^{133}Cs(\gamma,\pi^-xn)$ reaction is shown by adding all the values for x=0 to 9 at k=threshold to 500 MeV, and compared with three types of total photoabsorption cross sections. The largest contribution to the sum is from the reactions for $x=2\sim5$ including the estimated one for $^{133}Cs(\gamma,\pi^-3n)^{130}Ba$, as suggested from the mass yield curves shown in Fig. 3. The peak energy of the sum is 240 MeV and its FWHM is 90 MeV. The peak energies of the sum and the individual channels are far smaller than those expected from (3,3) resonance in pion photoproduction from a free nucleon (N). The total photoabsorption cross section σ_{tot} may be regarded to be a measure for the sum of the decay channels such as (γ,π^-xn), (γ,π^-xnyp), $(\gamma,\pi^{\pm,0}xnyp)$ and $(\gamma,xnyp)$. If σ_{tot} for a target of mass number A_t, is taken simply to be $A_t\cdot\sigma_{\gamma N}$, $\sigma_{\gamma N}$ being an average of the single nucleon total absorption cross section,[34] $\sigma_{\gamma N}=(\sigma_{\gamma p}+\sigma_{\gamma n})/2$, as an approximation, the sum of $^{133}Cs(\gamma,\pi^-xn)^{133-x}Ba$ is shown to be only 4% of $133\times\sigma_{\gamma N}$ (Fig. 8). It may be noteworthy that the present sum for (γ,π^-xn) would be (1.9 ± 0.6)% of the total hadronic cross section, $133\times\sigma_{\gamma h}$, which was obtained by Bonn, Mainz and Saclay groups and compiled by Ahrens and O'Connell[35] and Arends.[36] This may be more reasonably accounted for by comparing the total Ba yield of 1.6 mb/eq.q. with our preliminary photospallation yields of about 105 mb/eq.q. from ^{133}Cs(ref. 37). The difference of $\sigma_{\gamma N}$ and $\sigma_{\gamma h}$ suggests that photon is absorbed by dynamical assembly consisting of 133 nucleons. The total inelastic cross section (broken curve) obtained from the PICA code is in agreement at peak energy with both $\sigma_{\gamma N}$ and $\sigma_{\gamma h}$, if the PICA result (solid

curve) is shifted by 30 MeV as noted above in the comparison of the individual $\sigma(k)$ for the $(\gamma, \pi^- xn)$ reaction. The peak cross section and the width of the PICA result are still somewhat discrepant from $\sigma_{\gamma h} \cdot 133$.

It is now clear in Fig. 8 that the decay channel for $(\gamma, \pi^- xn)$ is actually the simplest part of (3,3) resonance absorption among others, being opened at the lowest excitation of the resonance absorption. The remaining channels end up in socalled spallation with and without pion emission. The PICA calculation indicates that the $(\gamma, xnyp)$, $(\gamma, \pi^0 xnyp)$, $(\gamma, \pi^- xnyp)$ and $(\gamma, \pi^+ xnyp)$ channels with $x, y \geq 0$ account for about 60, 20, 13 and 7%, respectively, of the total cross sections at k=200 to 400 MeV. Also it is indicated in PICA that the distribution of the points (R) where the emitting particles experience the last collision in the nucleus of radius (Ro) are from R/Ro=0.4 to 1 with a maximum at aound $R/Ro = 0.7 \sim 0.8$, which suggests that only the nucleons in the outer region of nucleus are involved in the reaction process and the particles produced in the central region are prohibitted to escape. This may, however, be understood to be a consequence of the assumption on density distribution, i.e. $\rho(R) = \alpha_i \rho(o)$, i=1, 2 and 3, where $\alpha_1 = 0.9$, $\alpha_2 = 0.2$ and $\alpha_3 = 0.01$. These results are identical with our similar comparison for $^{51}V(\gamma, \pi^- xn)^{51-x}Cr$.[7] In the case of ^{51}V, the total cross sections for the $(\gamma, \pi^- xn)$ reaction have its peak at 225 MeV and a FWHM of 90 MeV, and amount only to $(0.6 \pm 0.2)\%$ of the $51 \cdot \sigma_{\gamma h}$. Theoretical calculations based on valence nucleon model and/or, DWIA and PICA by the Lund group[3,6,9,10]

were available for ^{51}Ti and ^{49}Cr, but both the magnitude and shape of the calculated curves were in disagreement with our observation[7].

It is concluded that the observed features suggest that the photon reaction samples the entire nuclear volume, though the detailed accounts for whole kinematical and dynamical effects of the Δ-hole propagation in the nucleus[38], not only on charged pion-emitting reactions but on the other channels, are required for a more quantitative discussion, along with further systematic experiments.

ACKNOWLEDGMENTS

The authors are indebted to Drs. M. Yagi and K. Masumoto of the Laboratory of Nuclear Science, Tohoku University, Drs. T. Tomimasu and Y. Kawada of the Electrotechnical Laboratory, and Drs. K. Yoshida, T. Miyachi and M. Mutou of the Institute for Nuclear Study, University of Tokyo for their invaluable cooperations in accelerator operations and to Mr. T. Fukasawa and the other students of the Radiochemistry Laboratory of Kanazawa University in radioactivity measurements. Miss N. Fukushima is acknowledged for her typing and drawing. This work was supported by a Grant-in-Aid for Scientific Research (60430012) of the Ministry of Education, Science and Culture of Japan.

References

1 P.Stoler ed., "Photopion Nuclear Physics", (Plenum Press, N.Y. and London, 1979).

2 H.Arenhövel and D.Drechsel ed., "Nuclear Physics with Electromagnetic Interactions" Proc. Intern. Conf., in Mainz, Lecture Notes in Physics 108 (Springer-Verlag, Berlin, Heidelberg and N.Y., 1979).

3 G.Nydahl and B.Forkman, Nucl. Phys. B7, 97 (1968).

4 I.Blomqvist, G.Nydahl and B.Forkman, Nucl. Phys. A162, 193 (1971).

5 G.Kumbartzki and U.Kim, Nucl. Phys. A176, 23 (1971).

6 I.Blomqvist, P.Janecek, G.G.Jonsson, H.Dinter, K.Tesch, N. Freed and P.Ostrander, Phys. Rev. C 15, 988 (1977).

7 K.Sakamoto, M.Yoshida, T.Fukasawa, Y.Hamajima, S.Shibata and I.Fujiwara, Nucl. Phys. A (1989, in press).

8 R.A.Meyer and J.P.Hummel, Phys. Rev. 140, B48 (1965).

9 B.Bülow, B.Johnsson, M.Nilsson and B.Forkman, Z. Phys. A278, 89 (1976).

10 I.Blomqvist, P.Janecek, G.G.Jonsson, R.Petersson, H.Dinter, and K.Tesch, Z. Phys. A278, 83 (1976).

11 V.di Napoli, F.Salvett, M.L.Terranova, H.G.de Carvalho, J.B.Martins and O.A.P.Tavares, J. Inorg. Nucl. Chem. 40, 175 (1978).

12 I.Blomqvist, B.Bülow, A.Fredrikson, B.Johnsson, K.Lindgren, M.Nilsson, R.Petersson, O.Glomset, N.Freed and W.Rhodes, Z. Phys. A288, 313 (1978).

13 B.Bülow, B.Johnsson, G.G.Jonsson, K.Lindgren, M.Nilsson and R.Petersson, Z. Phys. A290, 393 (1979).

14 P.H.Ballentine, J.K.Hersh, H.A.Medicus, S.Planeta, F.Potentiani and S.Rossdentscher, in "Photopion Nuclear Physics", ed. P.Stoler, (1979) pp.387-389.

15 T.A.Gabriel and R.G.Alsmiller,Jr., Phys. Rev. 182, 1035 (1969).

16 T.A.Gabriel, M.P.Guthrie and O.W.Hermann, ORNL-4687 (1971).

17 K.Sakamoto, H.Toramoto, Y.Hamajima, K.Okada and M.Dohniwa, Radiochim. Acta 37, 69 (1984).

18 M.Sugawara, T.Ichinohe, S.Urasawa, M.Oyamada, T.Kubota, A.Karihara, O.Konno, Y.Shibazaki, T.Terasawa, K.Nakahara, S. Enomoto, M.Muto, K.Shoda and Y.Torizuka, Nucl. Instrum. Meth. 153, 343 (1978).

19 B.Johnsson, H.Harund and B.Forkman, Z. Phys. A273, 97 (1975).

20 K.Lindgren and G.G.Jonsson, Nucl. Phys. A166, 643 (1971).

21 K.Osada, T.Fukasawa, K.Kobayashi, Y.Hamajima, K.Sakamoto, S.Shibata and I.Fujiwara, Res. Rept. Lab. Nucl. Sci., *Tohoku Univ.* 20, 299 (1987).

22 K.Komura, Tech. Rept. Inst. Nucl. Study, Univ. Tokyo, INS-TCH-9 (1974).

23 U.Reus and W.Westmeier, Atomic Data and Nuclear Data Tables, 29, *Catalog of* Gamma Rays from Radioactive Decays, Pt.II, pp.193-406 (1983).

24 E.Browne and R.B.Firestone, "Table of Radioactive Isotopes" ed. V.S.Shirley (John Wiley & Sons, N.Y., 1986).

25 G.Andersson, P.Dougan and W.Stiefler, Z. Physl. A272, 263 (1975).

26 J.L.Matthews, W.Bertozzi, S.Kowalski, C.P.Sargent and W. Turchinetz, Nucl. Phys. A112, 654 (1968).

27 P.Dougan, B.Forkman, W.Stiefler and J.L.Matthews, Z. Phys. 269, 105 (1974).

28 K.Sakamoto, M.Dohniwa and K.Okada, Intern. J. Appl. Radiat. Isot. 36, 481 (1985).

29 M.Blann, Ann. Rev. Nucl. Sci. 25, 123 (1975).

30 F.Plasil, ORNL Report TM-6045 (1977).

31 K.Tesch, Nucl. Instrum. Meth. 95, 245 (1971).

32 J.T.Routi and J.V.Sandberg, Comput. Phys. Commu. 21, 119 (1980).

33 L.I.Schiff, Phys. Rev. 83, 252 (1951).

34 Particle Data Group, *Phys. Lett.* 170B, 85 (1986).

35 J.Ahrens and J.S.O'Connell, Comments Nucl. Part. Phys., 14, 245(1985).

36 J.Arends, Bonn-IR-88-05, Bonn University (1988) and refs. therein.

37 K.Sakamoto, Y.Hamajima, M.Soto, Y.Kubota, M.Yoshida, T. Hashimoto, T.Fukasawa, I.Fujiwara and S.Shibata, Res. Rep. Lab. Nucl. Sci., Tohoku Univ. 18, 290 (1985).

38 J.H.Koch, E.J.Moniz and N.Ohtsuka, Ann. Phys., 154, 99 (1984).

Captions of Figures

Fig. 1 The observed yields of Xe and Ba isotopes from ^{133}Cs as a function of maximum endpoint energy E_0 and the component analysis.

(a)~(i): the observed Ba yields shown by open circles are connected by a solid line. The inset is an expanded one in the threshold region. The broken line indicates the yields from the secondaries (see sec. C of the text for evaluation). The dotted line is the difference between the solid and broken lines and regarded to be the yield from $^{133}Cs(\gamma, \pi^- xn)^{133-x}Ba$.

(j): open circles with dotted error bars are for ^{133m}Xe and closed ones with solid bars are for ^{133g}Xe. Curves are to guide the eye. Secondary correction was unable due to insufficient data points.

Arrows on E_0 axis show the Q values for the secondary and photopion reactions. Q_n and Q_p refer to the neutron and proton-induced reactions, respectively.

Fig. 2 Depth profiles of yields in a thick target. A stack of CsCl disks with Al and Ni foils in between was irradiated with bremsstrahlung of E_0=800 MeV, and the radioactivities per unit weight were normalized to those of the front targets. Numbers in parentheses are the Q values in MeV for productions of indicated nuclides. Two entries in the parentheses for ^{131}Ba and ^{126}Ba are the Q values of $^{133}Cs(p,x'n)$ reactions (left) and of

$^{133}Cs(\gamma, \pi^- xn)$ reactions (right).

Fig. 3 Mass yield features of (γ, π^+) and $(\gamma, \pi^- xn)$ reactions on ^{133}Cs and ^{51}V targets at selected E_0. Averaged values are taken for E_0=400 to 1050 MeV. Closed symbols connected with solid curves are for the ground state isomers and the open ones with dotted curves (only for ^{133}Cs target) are for the metastable isomers. The values at x=0 on left is for (γ, π^+) and at x=0 on right and x=1 to 7 are for $(\gamma, \pi^- xn)$. The ^{133}Xe value is an upper limit for the (γ, π^+). The data on ^{51}V are from ref. 7.

Fig. 4 Cross sections $\sigma(k)$, in unit of μb per photon, as a function of photon energy k, obtained by unfolding of the yield curves of Fig. 1. (a) for the isomeric pairs and (b) for the ground state isomers. The broken curves show the $\sigma(k)$ for $^{133g,132,130,125}Ba$ estimated by interpolation of peak energies, FWHM and FWTM of the cross section curves. The unfolding was based on Schiff spectrum for bremsstrahlung and the smoothed yield curves as shown by the dotted ones in Fig. 1. Uncertainty in magnitude is estimated to be about 30% from the range of scattering of the observed data and that in peak energy is to be less than about 10 MeV.

Fig. 5 Variation of peak energies of the excitation curves for the photopion reactions on ^{133}Cs and ^{51}V as a function

of neutron multiplicity x.

Fig. 6 Comparison of the calculated $\sigma(k)$ by PICA code (symbols with statistical errors ; dotted curves to guide the eye) with the experimental ones (solid curves). (a) for the even mass products, ^{132}Ba (square), ^{130}Ba (triangle), ^{128}Ba (circle) and ^{126}Ba (cross), and (b) for the odd mass products ; ^{133}Xe (closed circle), ^{133}Ba (reversed triangle), ^{131}Ba (egg), ^{129}Ba (diamond) and ^{127}Ba (star). The calculation resulted only a single value (30 ±17)mb at 300 MeV for ^{124}Ba in the particle history of $(0.2\sim1)\cdot10^{6}$, not shown in the figure. The photon energy scale for the PICA results is shown in parenthesis and those for the experimental ones without parenthesis.

Fig. 7 Peak cross sections as a function of neutron multiplicity x for ^{133}Cs(γ , π^{-}xn)$^{133-x}$Ba, as depicted from Fig. 6. The PICA code results an odd-even effect as shown by a broken curve for the even mass products (x=odd) and a one-dot broken one for the odd mass products (x=even). The closed circles tied by a solid curve is from the present experiment.

Fig. 8 Sum of $\sigma(k)$ for formation of $^{133-x}$Ba from ^{133}Cs(γ , π^{-}xn) reaction for x≤9 and three types of the total photoabsorption cross sections. The total photo-

absorption cross section was first approximated simply by $A_t \cdot \sigma_{\gamma N}$ A_t(=133) being target mass and $\sigma_{\gamma N}$ = ($\sigma_{\gamma p}$+ $\sigma_{\gamma n}$)/2 being an average of single nucleon total photoabsorption cross sections,[33] and shown by a dotted curve. The shaded area is the range of the total hadronic cross sections, $\sigma_{\gamma h}$ per nucleon,[34,35] multiplied by 133. Total cross sections from the PICA calculation is shown by a solid curve as indicated. The broken one is the PICA result shifted by 30 MeV in energy scale (see also Fig. 6). The small solid curve is the sum of the ^{133}Cs(γ , π^- xn) cross sections of x=0 to 9 of Fig. 4(b).

Table 1 Relevant nuclear data for yield measurements

Nuclide	Half-life	γ-Ray energy measured (keV)	Fractional abundance (%)
Ba-133m	38.9 h	276.1	17.5
Ba-131m	14.6 m	108.5	55.2
Ba-131g	11.8 d	496.3	47.1
Ba-129m	2.13 h	182.3	47.0
Ba-129	2.16 h	411.5	22.7
Ba-128	2.43 d	273.4	14.5
Ba-127	12.7 m	114.8	9.26
Ba-126	1.67 h	233.6	20.4
Ba-124	11.9 m	169.5	21
Cs-129	32.1 h	371.9	31.1
Xe-133m	2.19 d	233	9.95
Xe-133g	5.29 d	81	35.9
Xe-123	2.08 h	148.9	48.6
Na-24	15.02 h	1368.5	100
Au-196	6.18 d	355.7	86.9

Table 2 Measured yields of Ba isotopes from ^{133}Cs in unit of μb per equivalent quanta (μb/eq.q.)

Eo (MeV)	^{130m}Ba	$^{131g+m}$Ba	^{132}Ba	^{133m}Ba	^{133g}Ba	^{135m}Ba	^{136m}Ba
1050	65.7 ± 6.6	262 ± 34	336 ± 36	168 ± 15	387 ± 36	306 ± 28	
	74.1 ± 10.5	179 ± 35	304 ± 49	198 ± 25	366 ± 51	314 ± 43	
1000	58 ± 5.8	284 ± 12	251 ± 27	143 ± 10	311 ± 18	232 ± 32	
	57.6 ± 8.3	173 ± 16	3.1 ± 26	157 ± 15	335 ± 33	230 ± 32	
	80.3 ± 7.3	196 ± 11	465 ± 28	255 ± 15	446 ± 46	337 ± 29	
950	80.0 ± 10.1	290 ± 8	338 ± 42	215 ± 4	466 ± 41	300 ± 20	
900	38.2 ± 10.3	136 ± 11	332 ± 7	162 ± 6	252 ± 41	269 ± 33	
850	63.0 ± 5.1	220 ± 12	385 ± 20	199 ± 12	437 ± 25	293 ± 29	
800	78.2 ± 3.3	146 ± 14	325 ± 14	182 ± 6	371 ± 16	303 ± 13	
	77.9 ± 3.5	288 ± 7	285 ± 10	218 ± 8	336 ± 11	336 ± 10	
		198 ± 16	456 ± 49	281 ± 23	513 ± 76	381 ± 45	
750	81.2 ±22.5	256 ± 23	333 ± 42	202 ± 26	284 ± 44	252 ± 48	
700	74.9 ± 9.0	305 ± 6	245 ± 8	159 ± 2	180 ± 14	219 ± 36	
	62.0 ± 12	146 ± 10	316 ± 21	168 ± 12	220 ± 28	235 ± 27	
650	42.9 ± 5.7	185 ± 17	320 ± 28	171 ± 16	302 ± 29	278 ± 26	
600	38.4 ±17.8	172 ± 9	273 ± 22	140 ± 7	280 ± 44	203 ± 11	
550	76.5 ±11.9	184 ± 15	320 ± 20	168 ±10	292 ± 30	281 ± 38	
500	50.8 ±23.3	191 ± 22	295 ± 27	132 ± 15	444 ± 68	243 ± 65	
	72.1 ± 6.6	216 ± 20	295 ± 28	152 ± 12	318 ± 35	253 ± 23	
	57.8 ± 4.7	209 ± 12	339 ± 10	146 ± 7	325 ± 15	261 ± 18	
		240 ± 30	486 ±51	232 ± 28	352 ± 49	239 ± 49	
450	59.5 ± 8.8	208 ± 30	371 ± 22	179 ± 15	367 ± 48	288 ± 34	
400	37.8 ±23.8	118 ±48	303 ± 45	198 ± 8	140 ± 82	176 ± 11	
	36.5 ± 9.8	197 ± 6	275 ± 9	165 ± 6	273 ± 26	232 ± 11	
350	34.2 ± 8.8	148 ± 5	241 ± 16	123 ± 4	282 ± 24	162 ± 27	
320		191 ± 13	321 ± 41	160 ± 15	288 ± 45		
305	48.2 ± 2.4	88.5 ± 2.8	173 ± 5	88.2 ± 2.4	137 ± 6	107 ± 4	
	38.2 ± 3.2		157 ± 5	88.3 ± 2.8	112 ± 8	84 ± 7.7	
	49.2 ± 1.8	113 ± 7	203 ± 4	94.2 ± 2.8	160 ± 7	123 ± 5	
	38.6 ± 1.4		188 ± 2	76.3 ± 1.5		96.5 ± 3.2	
300	42.2 ± 4.9	124 ± 4	225 ± 12	115 ± 8	259 ± 16	168 ± 11	
250	41.6 ± 2.0	65.2 ± 1.8	154 ± 4	66.8 ± 1.2	98.6 ± 7.8	94.6 ± 2.2	
	47.4 ± 2.4	81.3 ±28.8	168 ±10	98.8 ± 3.3		82.5 ± 6.1	
230	29.8 ± 1.9	60.5 ± 4.1	89.2 ± 8.6	21.1 ± 1.4	58.1 ± 2.8	16.9 ± 1.3	
220	25.8 ± 2.8	46.7 ± 1.8	86.8 ± 3.2	19.3 ± 0.7		15.2 ± 1.2	
	23.3 ± 8.3	48.8 ± 8.6	80.5 ± 1.4	22.8 ± 8.2	22.8 ± 8.3	8.85 ± 8.25	
210	26.4 ± 1.8	47.8 ± 2.7	81.6 ± 6.6	11.2 ± 8.8	38.3 ± 1.1	5.85 ± 8.55	
195	17.2 ± 8.8	27.4 ± 8.6	54.1 ± 1.6	3.48 ± 8.11	5.38 ± 8.28	1.83 ± 8.26	
175	10.3 ± 8.2	12.8 ± 8.3	17.4 ± 8.8	1.83 ± 8.42	3.13 ± 8.23	1.39 ± 8.88	
160	8.81 ± 8.85	7.27 ± 8.49	12.1 ± 8.7	1.53 ± 8.88		8.95 ± 8.17	
150	3.59 ± 8.41	5.22 ± 8.66	7.56 ± 8.87	8.79 ± 8.88	3.38 ± 8.15	8.52 ± 8.86	
145	3.78 ± 8.19	5.88 ± 8.15	8.85 ± 8.35	1.83 ± 8.84	2.87 ± 8.89	8.76 ± 8.86	
140	4.23 ± 8.13	6.66 ± 8.17	11.2 ± 8.58	1.18 ± 8.83	2.88 ± 8.87	8.88 ± 8.84	
138	3.36 ± 1.87	4.35 ± 1.34	7.17 ± 2.25	8.61 ± 8.18			
134	4.28 ± 8.21	3.68 ± 8.19	6.89 ± 8.57	8.317 ± 8.823	8.67 ± 8.13	8 ± 8.814	
128	2.64 ± 8.31	2.84 ± 8.33	5.18 ± 8.48	8.258 ± 8.838			
65	1.57 ± 8.83	8.86 ± 8.81	1.18 ± 8.82	8.8838± 8.8883	8.887± 8.884	8 ± 8.811	
64	1.29 ± 8.82	8.58 ± 8.87	8.98 ± 8.36	8 ± 8.8888	8 ± 8.818	8 ± 8.21	
55	1.25 ± 8.88	8.28 ± 8.81	8.52 ± 8.85	8 ± 8.8848	8 ± 8.852	8 ± 8.89	
45	8.69 ± 8.87	8.858 ± 8.885	8.878 ± 8.81	8 ± 8.8889	8 ± 8.838	8 ± 8.825	
40	8.65 ± 8.82	8.321 ± 8.881	8.815 ± 8.887	8 ± 8.8839	8 ± 8.852	8 ± 8.854	
38	8.21 ± 8.82	8 ± 8.88/2	8 ± 8.86	8 ± 8.8887	8 ± 8.883	8 ± 8.818	

Table.2 Continued

Eo (MeV)	^{137}Ba	^{138}Ba	^{134}Ba	^{133m}Xe	^{133}Xe
1050	106 ± 11	75.7 ± 6.6	11.4 ± 4.4	———	———
	120 ± 17	90.0 ± 11.3	14.7 ± 3.9	———	———
1000	115 ± 11	74.9 ± 4.8	———	———	———
	———	84.6 ± 6.1	———	17.5 ± 9.5	26.2 ± 4.6
	146 ± 12	120.6 ± 7.0	16.3 ± 1.7	———	———
950	168 ± 8	95.9 ± 4.3	15.3 ± 2.7	———	———
900	———	75.6 ± 9.9	———	34.0 ± 10.0	47.0 ± 46.0
850	136 ± 12	85.3 ± 5.0	12.0 ± 3.8	———	———
800	162 ± 15	78.6 ± 2.8	———	———	———
	133 ± 26	102 ± 6	———	13.1 ± 1.0	17.6 ± 1.1
	139 ± 12	134 ± 13	12.5 ± 1.6	———	———
750	149 ± 22	85.3 ± 12.0	13.0 ± 2.0	———	———
700	———	61.6 ± 3.6	———	11.8 ± 6.0	39.0 ± 23.0
	———	74.3 ± 4.0	———	———	———
650	112 ± 32	77.5 ± 7.5	11.8 ± 4.5	———	———
600	———	75.2 ± 3.6	———	———	———
550	149 ± 16	84.2 ± 7.3	18.7 ± 3.5	———	———
500	131 ± 6	71.0 ± 7.2	———	18.0± 27.0	32.0 ± 26.0
	137 ± 33	76.1 ± 7.2	———	———	———
	174 ± 36	79.8 ± 2.3	———	———	———
	192 ± 22	96.4 ± 11.2	16.7 ± 4.5	———	———
450	175 ± 28	62.0 ± 15.6	———	———	———
400	124 ± 9	59.1 ± 5.3	———	———	———
	———	71.2 ± 2.1	———	———	———
350	109 ± 12	43.6 ± 3.4	3.26 ± 2.11	———	———
330	100 ± 9.0	41.6 ± 4.7	4.7 ± 3.8	———	———
305	———	21.3 ± 0.8	———	———	———
	———	26.7 ± 1.6	———	———	———
	———	33.2 ± 1.1	———	———	———
	———	22.1 ± 1.5	———	———	———
300	62.3 ± 5.2	31.0 ± 2.0	———	———	10.9 ± 1.4
250	———	2.52 ± 0.12	———	———	———
	———	3.83 ± 0.22	———	———	———
230	2.58 ± 0.26	0.95 ± 0.05	———	———	———
220	———	1.31 ± 0.08	———	———	———
	1.79 ± 0.54	0.39 ± 0.03	0.028 ± 0.237	———	———
210	0.91 ± 0.23	———	———	———	———
195	0.452± 0.08	0.119 ± 0.025	———	———	———
175	0.236± 0.024	0.065 ± 0.011	———	———	———
160	———	0 ± 0.222	———	———	———
150	0.115± 0.020	0.007 ± 0.002	———	———	———
145	———	0.016 ± 0.012	———	———	———
140	0.110± 0.013	0.019 ± 0.009	0.007 ± 0.16	———	———
130	———	0 ± 0.205	———	———	———
104	———	0 ± 0.017	———	———	———
100	———	0 ± 0.11	———	———	———
65	———	0 ± 0.020	———	———	———
64	———	0 ± 0.0091	———	———	———
55	———	0 ± 0.028	———	———	———
45	———	0 ± 0.014	———	———	———
40	———	0 ± 0.054	———	———	———
30		0 ± 0.0012	———	———	———

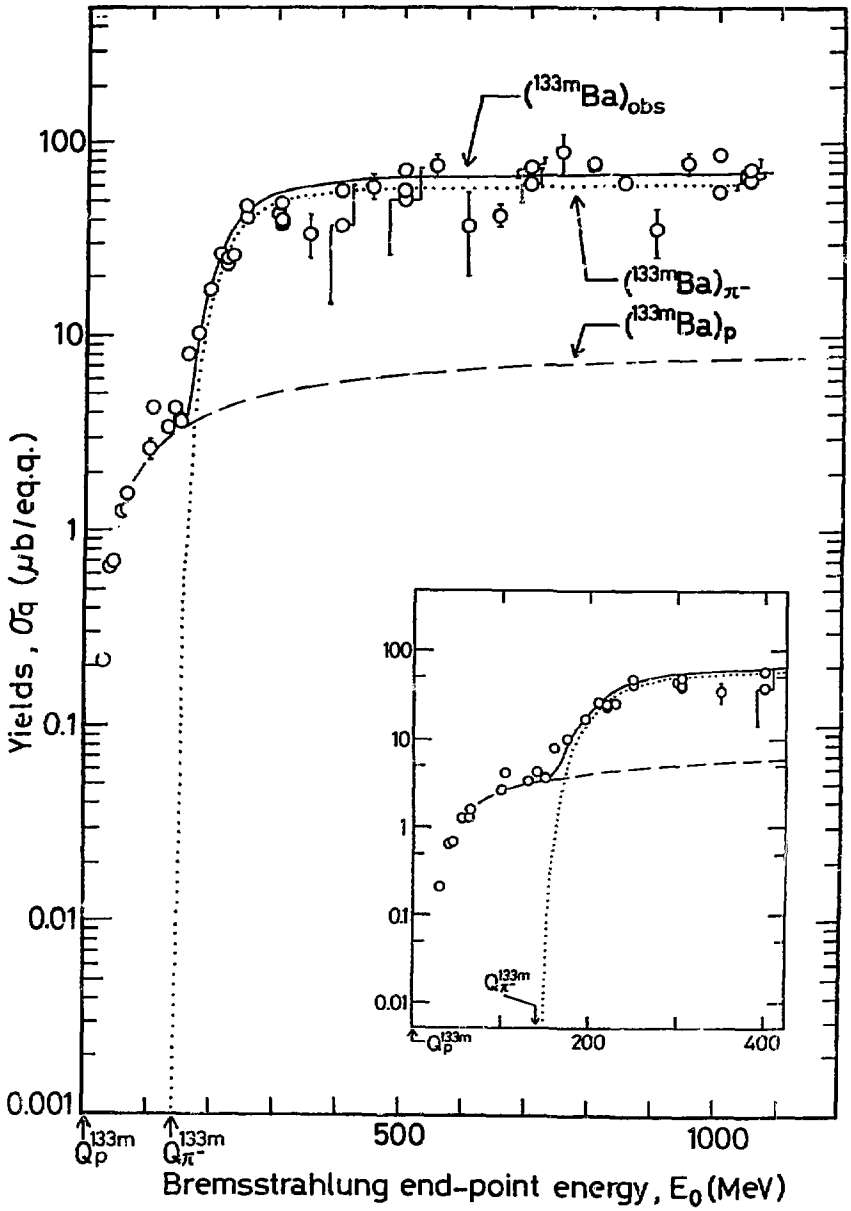
$(^{133m}Ba)_{obs}$
$(^{133m}Ba)_{\pi^-}$
$(^{133m}Ba)_p$
Yields, σ_q (μb/eq.q.)
100
10
1
0.1
0.01
0.001
Q_p^{133m}
$Q_{\pi^-}^{133m}$
500
1000
Bremsstrahlung end-point energy, E_0 (MeV)
200
400

Fig. 1(a)

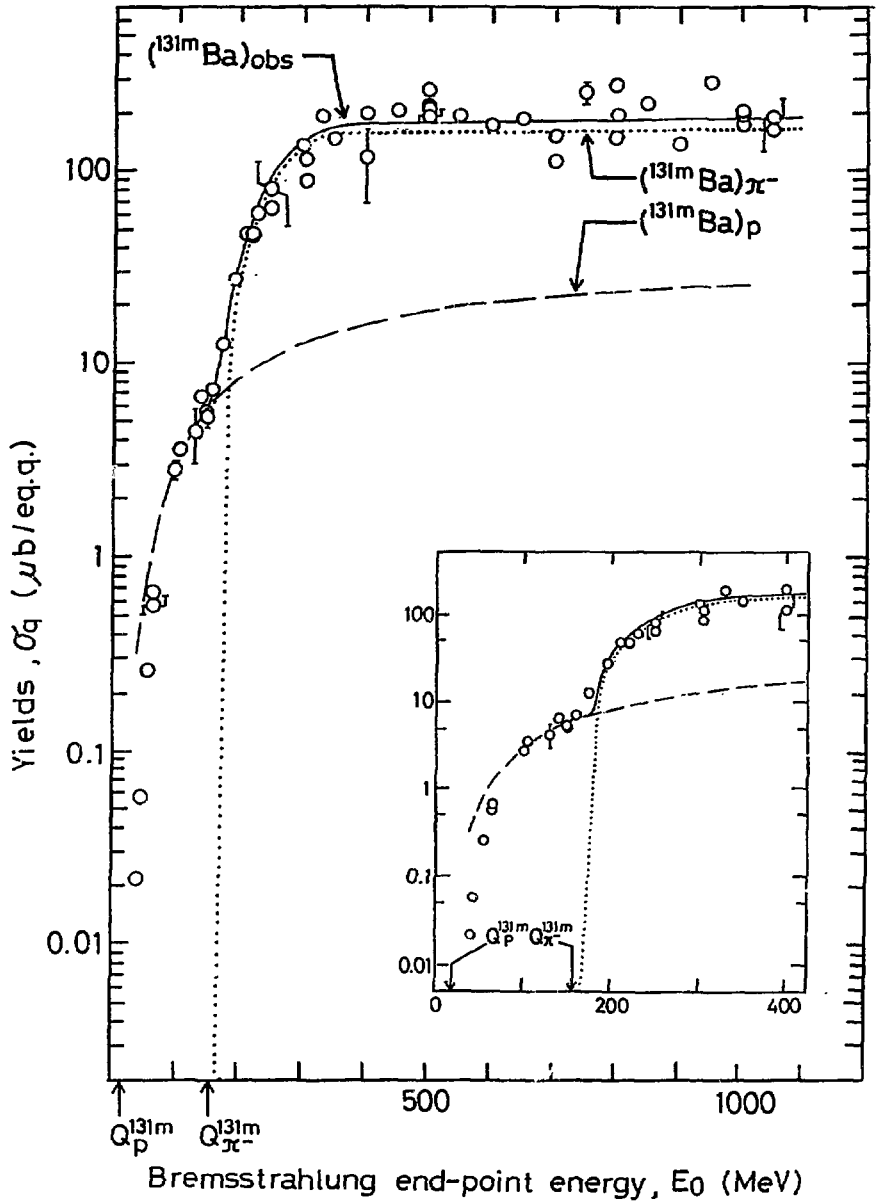
(131mBa)obs
(131mBa)π⁻
(131mBa)p
100
10
1
0.1
0.01
Yields , σq (μb/eq.q.)
500
1000
Q131mp
Q131mπ⁻
Bremsstrahlung end-point energy, E0 (MeV)
100
10
1
0.1
0.01
0
200
400
θ
Q131mp Q131mπ⁻

Fig. 1(b)

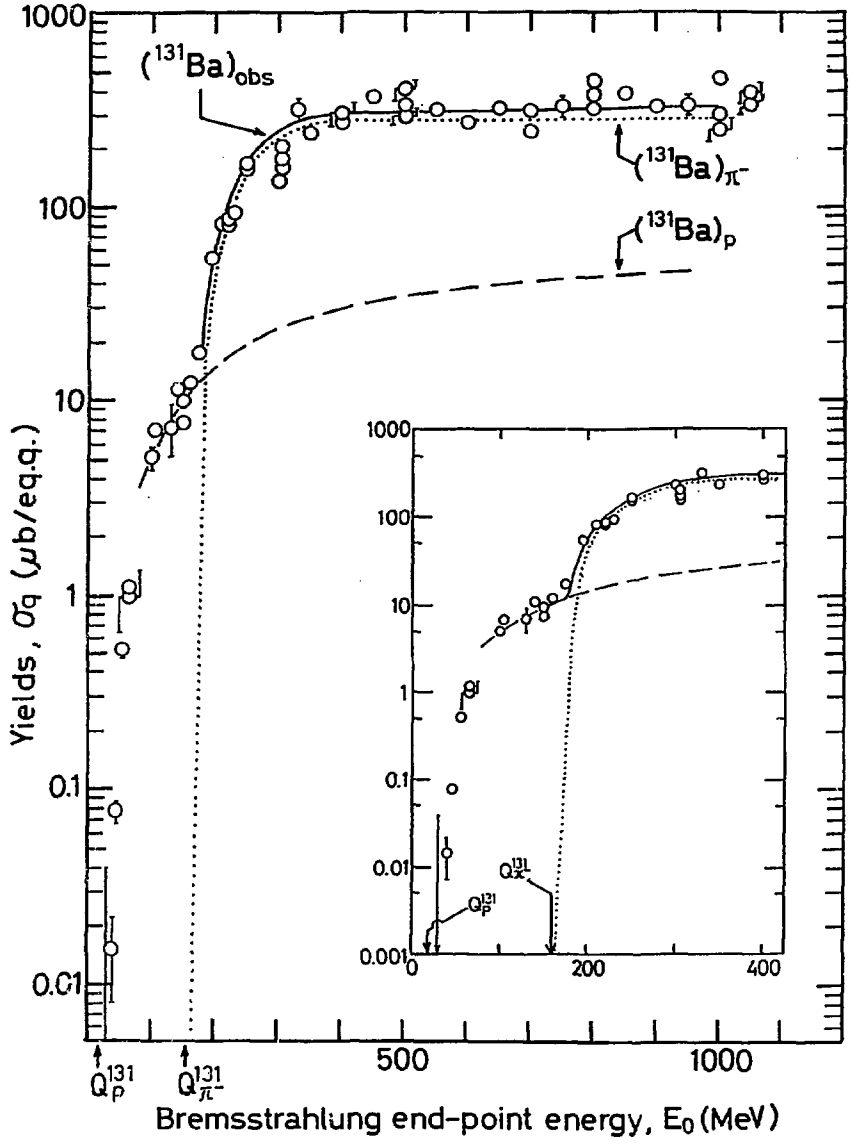
1000
100
10
1
0.1
0.01
$(^{131}Ba)_{obs}$
$(^{131}Ba)_{\pi^-}$
$(^{131}Ba)_p$
Yields, σ_q (μb/eq.q.)
Q_p^{131}
$Q_{\pi^-}^{131}$
500
1000
Bremsstrahlung end-point energy, E_0 (MeV)
0.001
0
200
400
Q_x^{131}

Fig. 1(c)

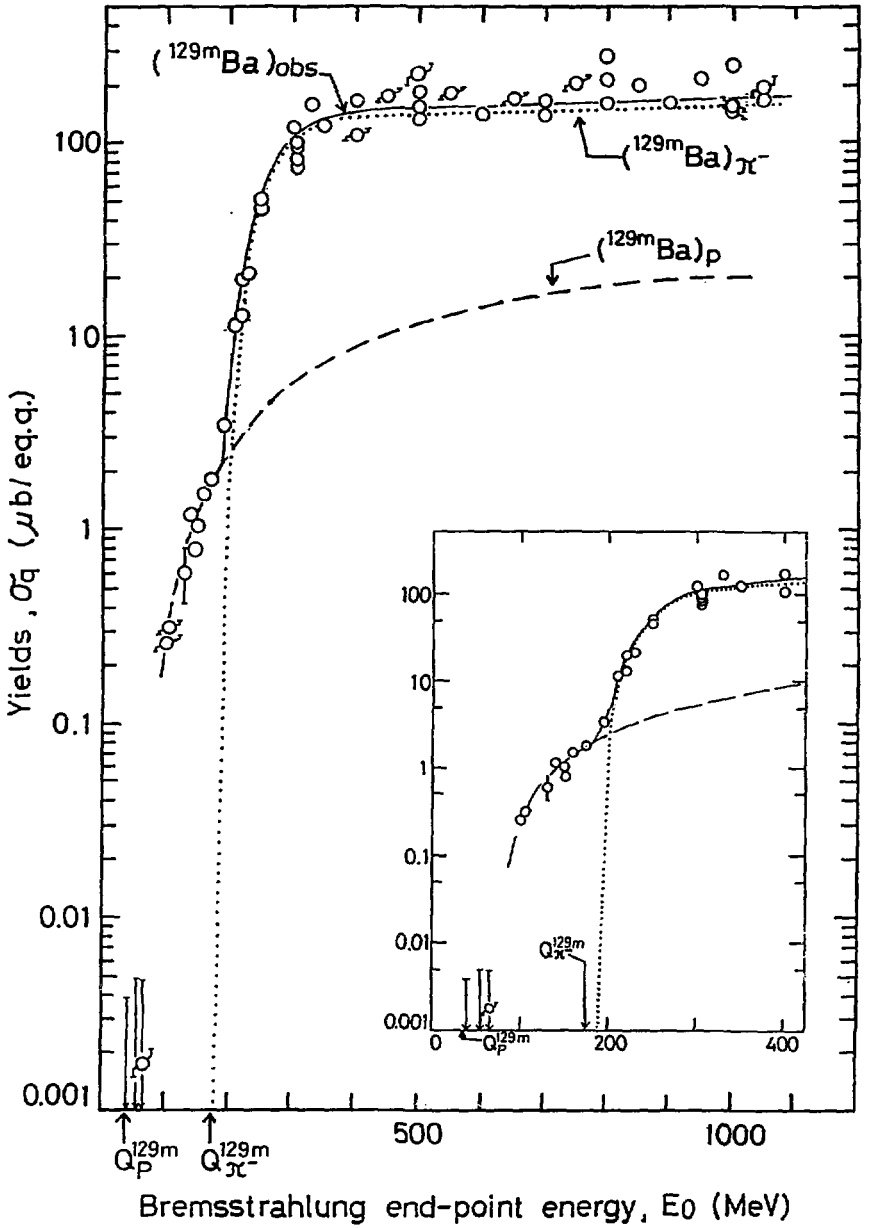
(129mBa)obs
(129mBa)π⁻
(129mBa)p
Yields , σq (μb/ eq.q.)
100
10
1
0.1
0.01
0.001
500
1000
Q_P^129m
Q_π⁻^129m
Bremsstrahlung end-point energy, E0 (MeV)
0
200
400

Fig. 1(d)

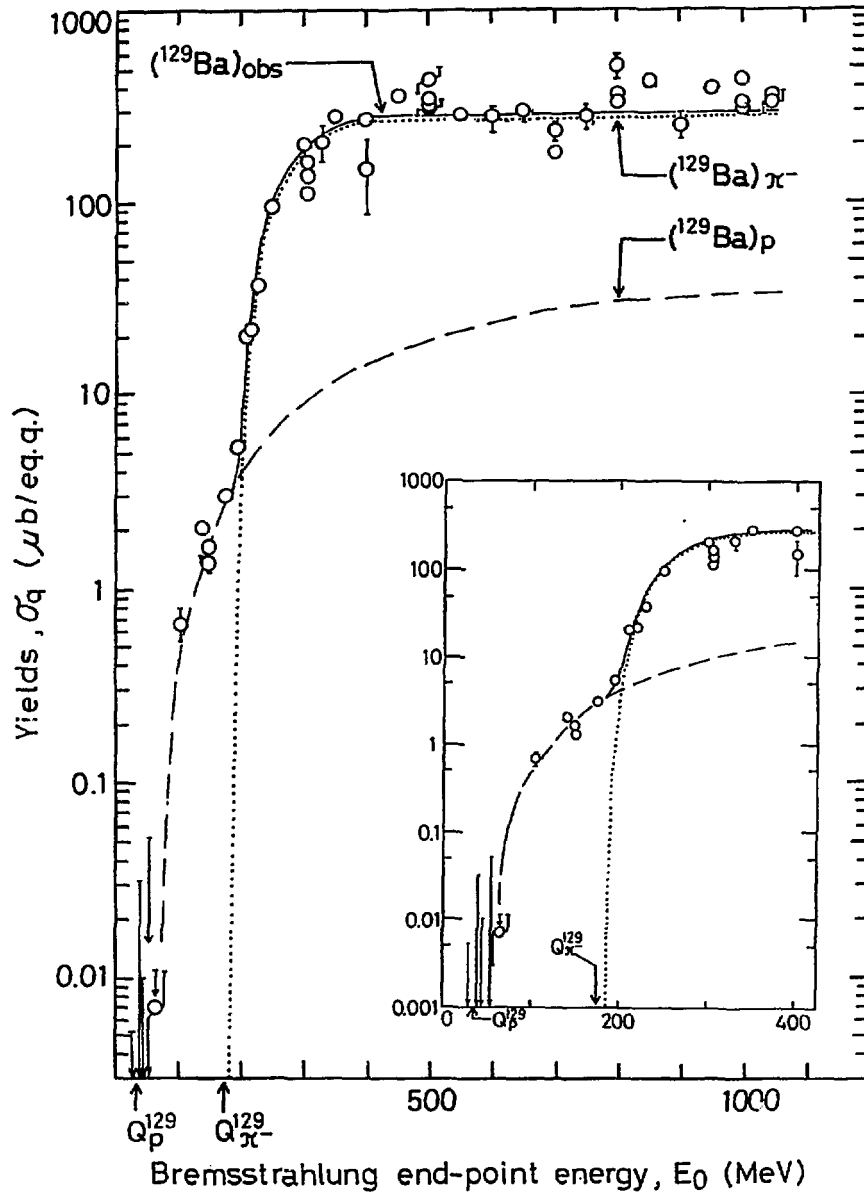
1000
100
10
1
0.1
0.01
(129Ba)obs
(129Ba)π⁻
(129Ba)p
Yields , σq (μb/eq.q.)
Q_p^129
Q_π⁻^129
500
1000
Bremsstrahlung end-point energy, E0 (MeV)
0.001
0
200
400

Fig. 1(e)

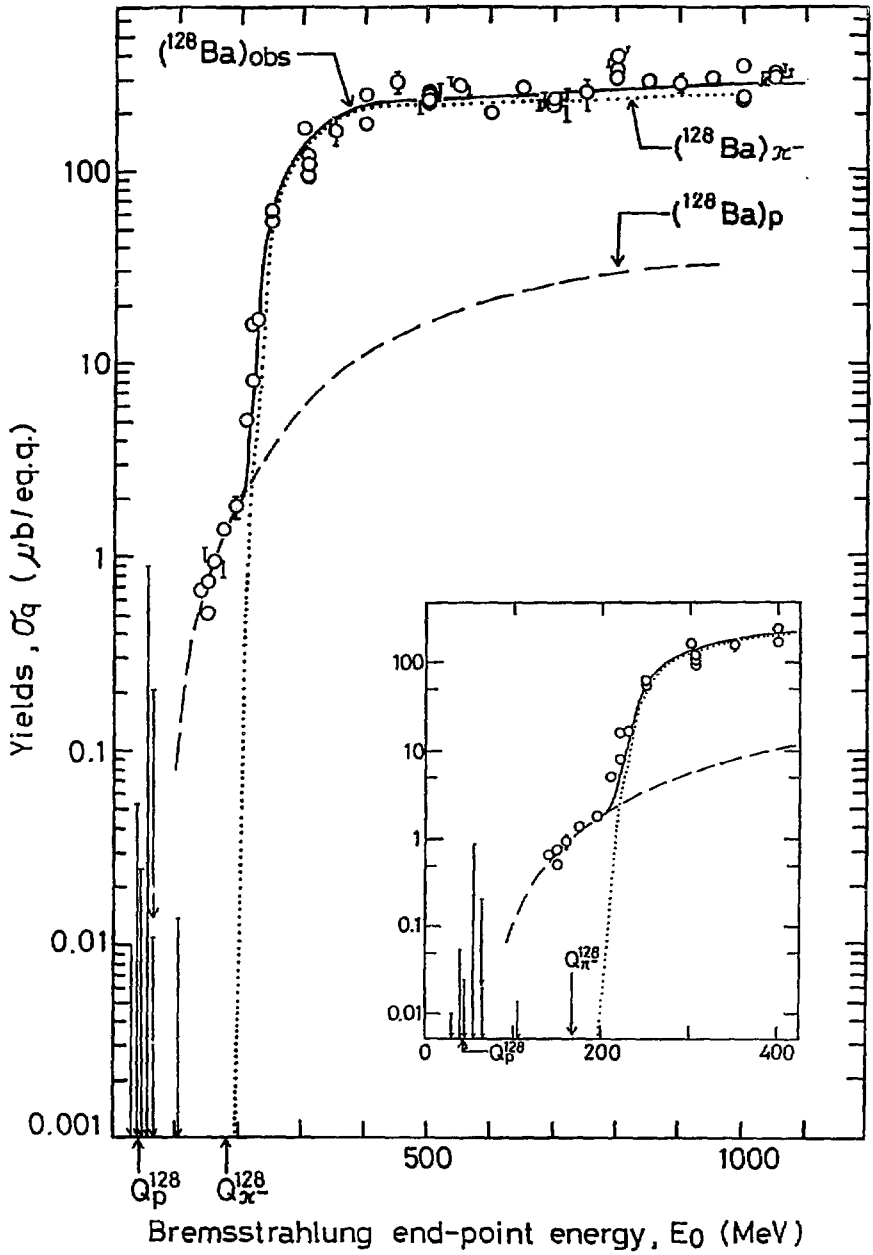
(128Ba)obs
(128Ba)π⁻
(128Ba)p
100
10
1
0.1
0.01
0.001
Yields, σq (μb/eq.q.)
500
1000
Q_p^128
Q_π⁻^128
Bremsstrahlung end-point energy, E0 (MeV)
100
10
1
0.1
0.01
0
200
400
Q_p^128
Q_π^128

Fig. 1(f)

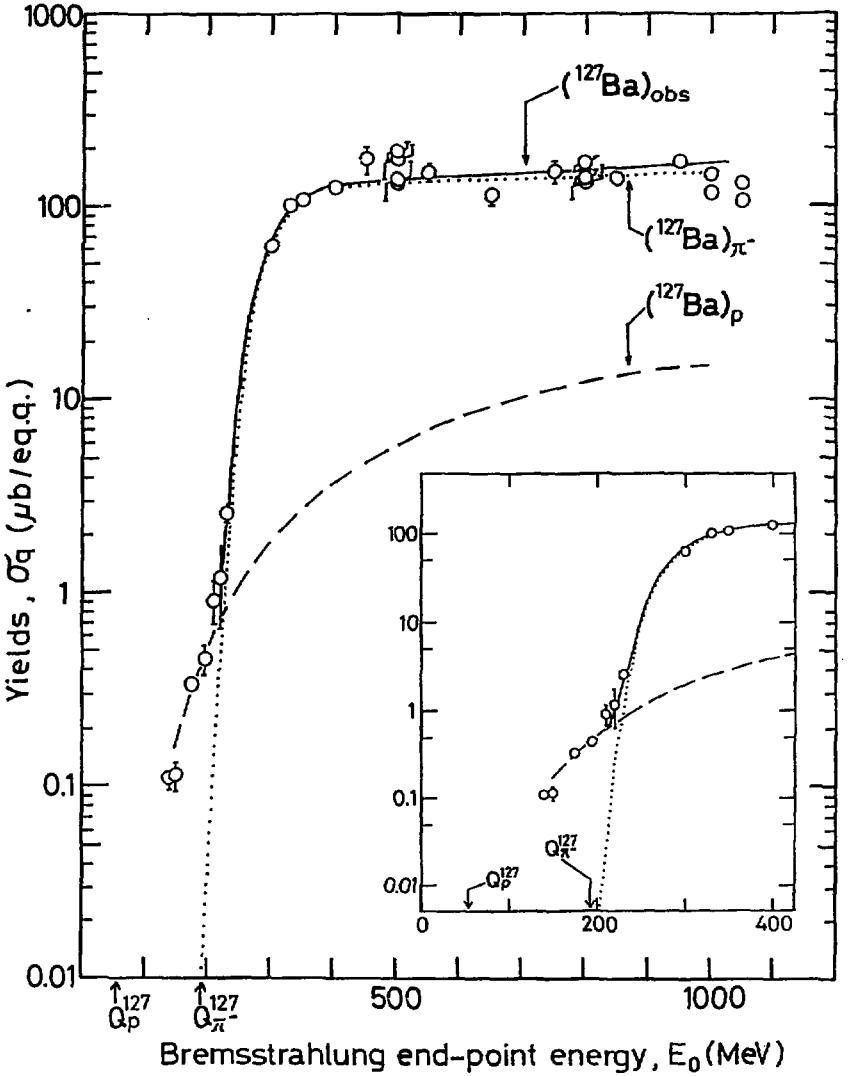
1000
100
10
1
0.1
0.01
Yields, σq (μb/eq.q.)
(127Ba)obs
(127Ba)π-
(127Ba)p
100
10
1
0.1
0.01
0
200
400
Q127p
Q127π-
500
1000
Bremsstrahlung end-point energy, E0 (MeV)

Fig. 1(g)

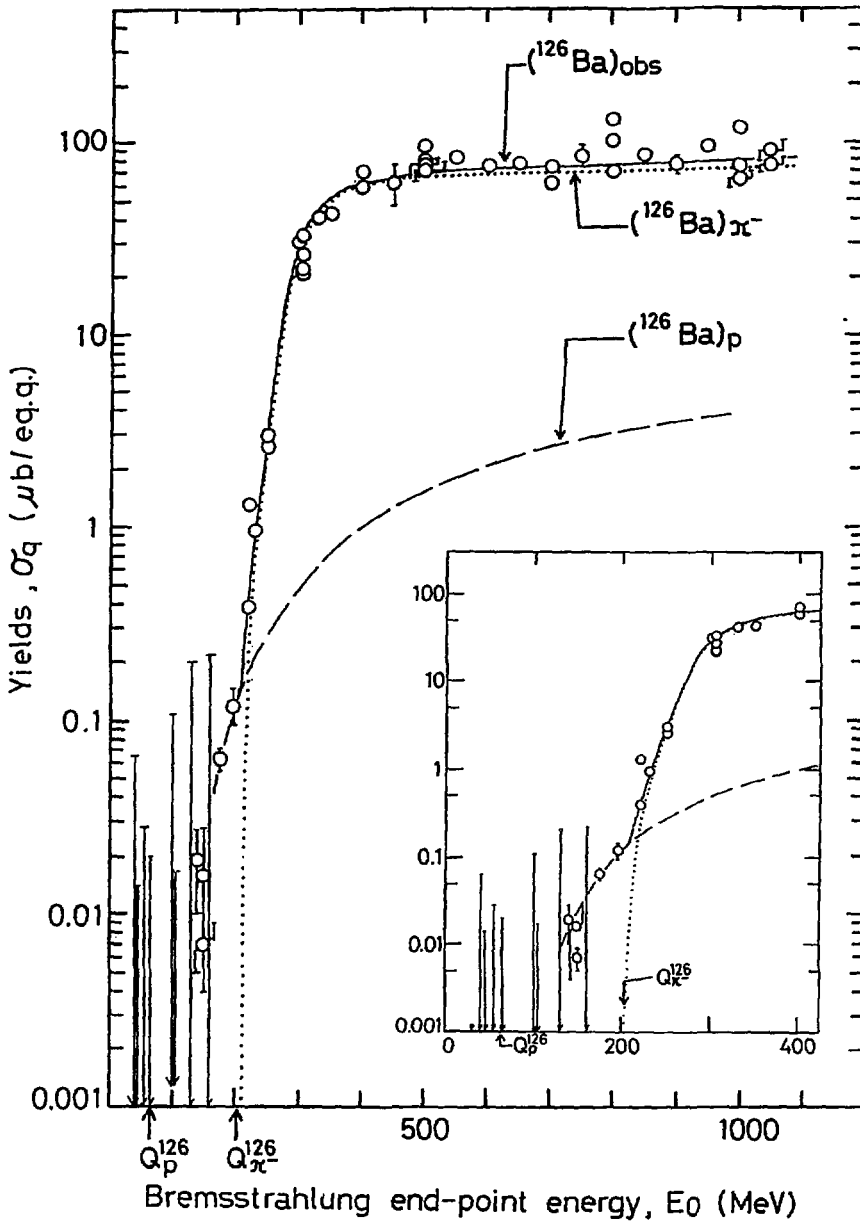
(126Ba)obs
(126Ba)π⁻
(126Ba)p
Yields , σq (μb/eq.q.)
100
10
1
0.1
0.01
0.001
500
1000
Q_p^126
Q_π⁻^126
Bremsstrahlung end-point energy, E0 (MeV)
0
200
400

Fig. 1(h)

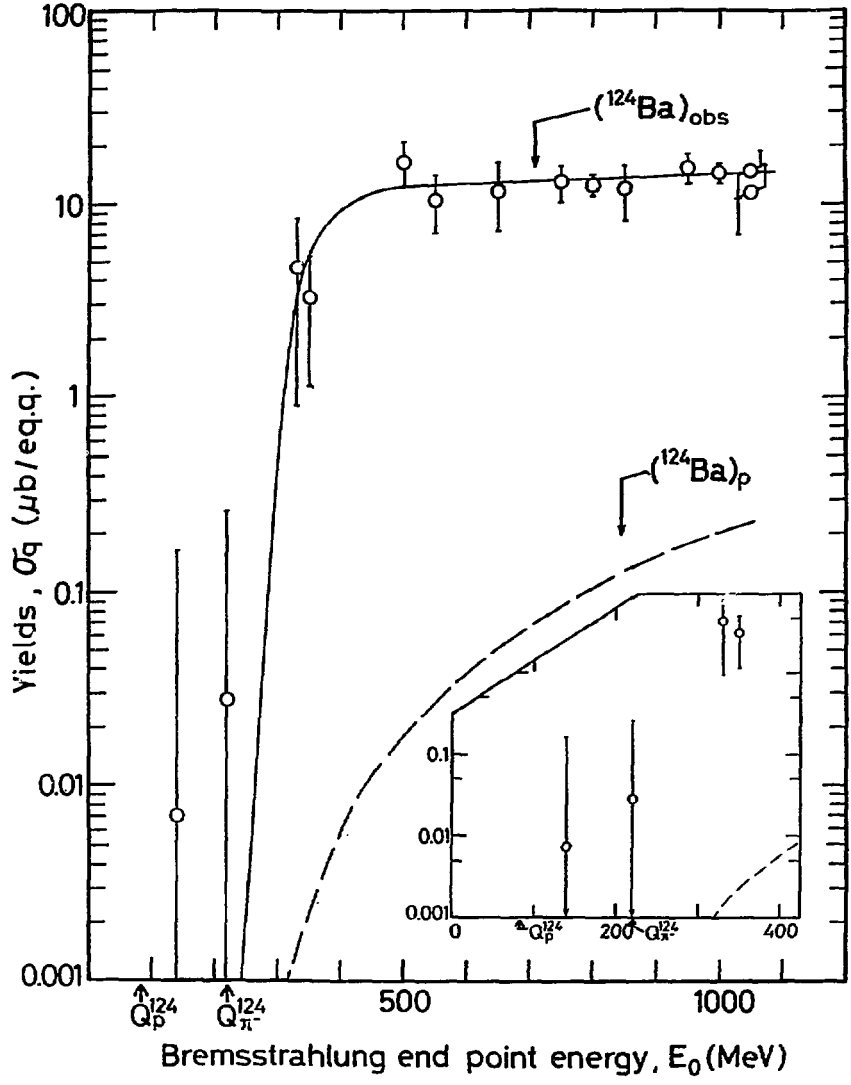
100
10
1
0.1
0.01
0.001
Yields, σ_q (μb/eq.q.)
$(^{124}Ba)_{obs}$
$(^{124}Ba)_p$
0.1
0.01
0.001
0
Q_p^{124}
200
$Q_{\pi^-}^{124}$
400
Q_p^{124}
$Q_{\pi^-}^{124}$
500
1000
Bremsstrahlung end point energy, E_0 (MeV)

Fig. 1(i)

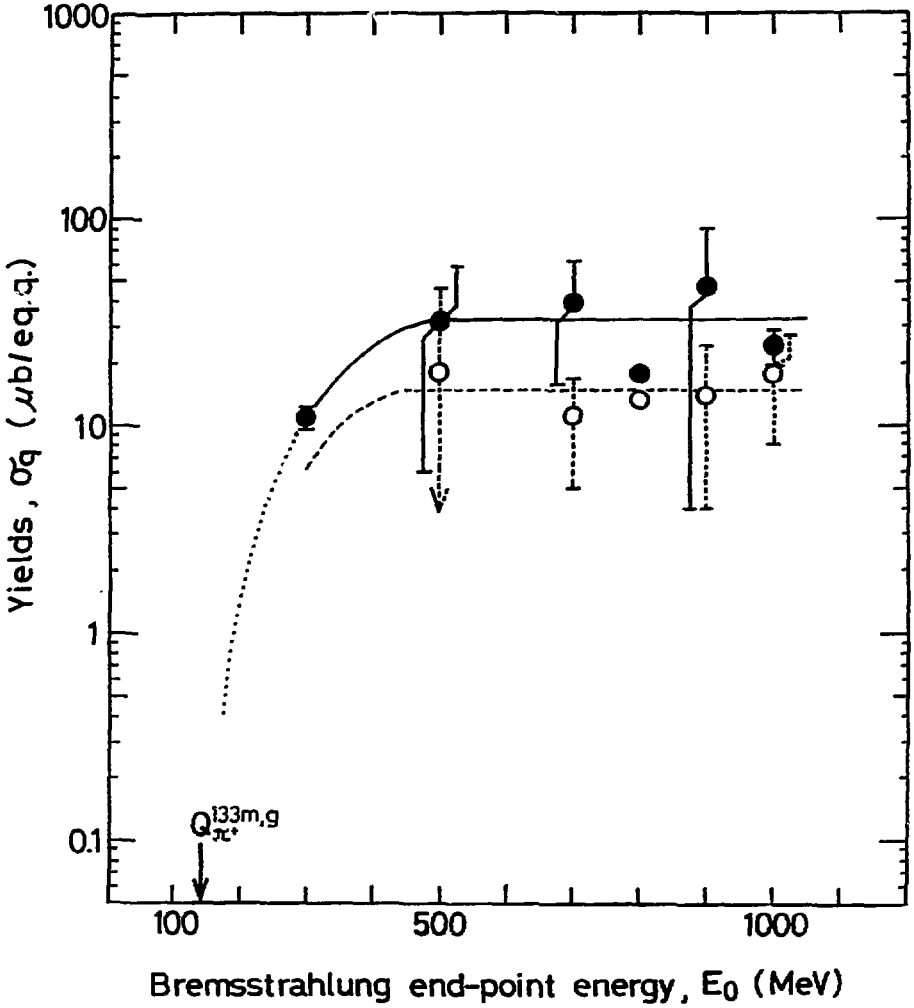
1000
100
10
1
0.1
Yields, σq (μb/eq.q.)
$Q_{\pi^+}^{133m,g}$
100
500
1000
Bremsstrahlung end-point energy, E_0 (MeV)

Fig. 1(j)

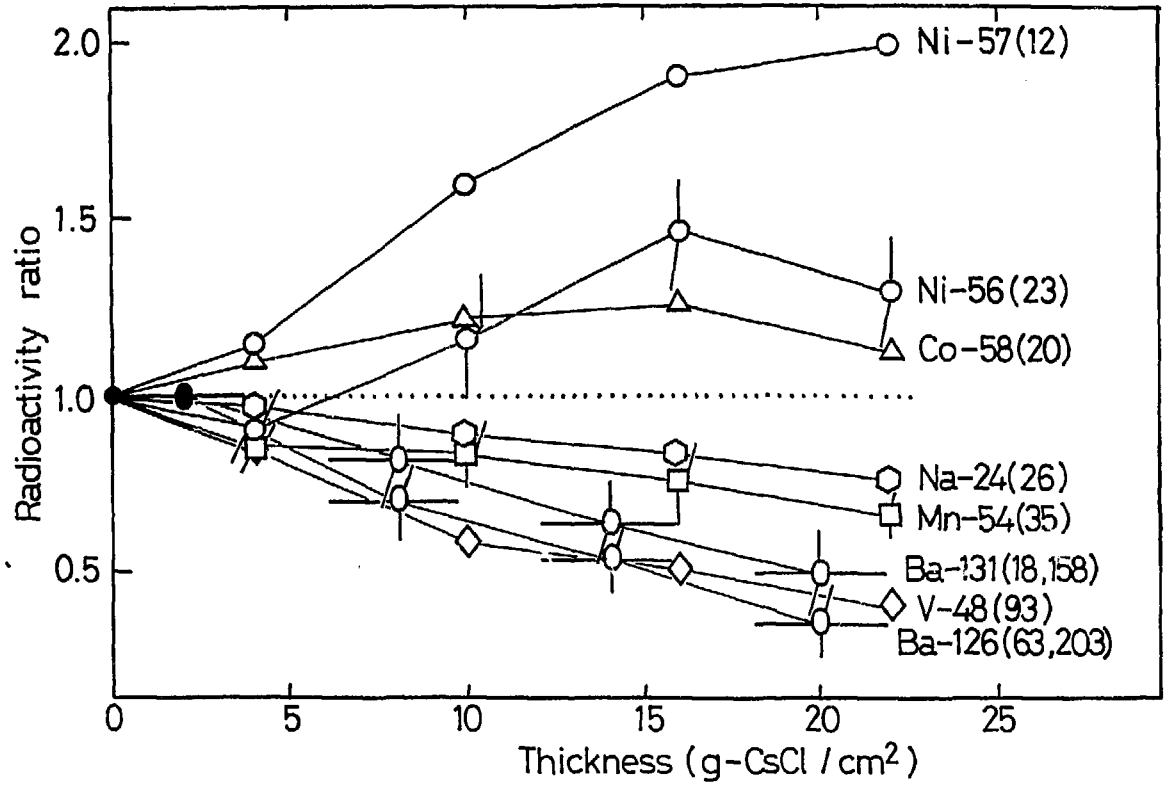
2.0
1.5
1.0
0.5
Radioactivity ratio
0
5
10
15
20
25
Thickness (g-CsCl / cm²)
Ni-57(12)
Ni-56(23)
Co-58(20)
Na-24(26)
Mn-54(35)
Ba-131(18,158)
V-48(93)
Ba-126(63,203)

Fig. 2

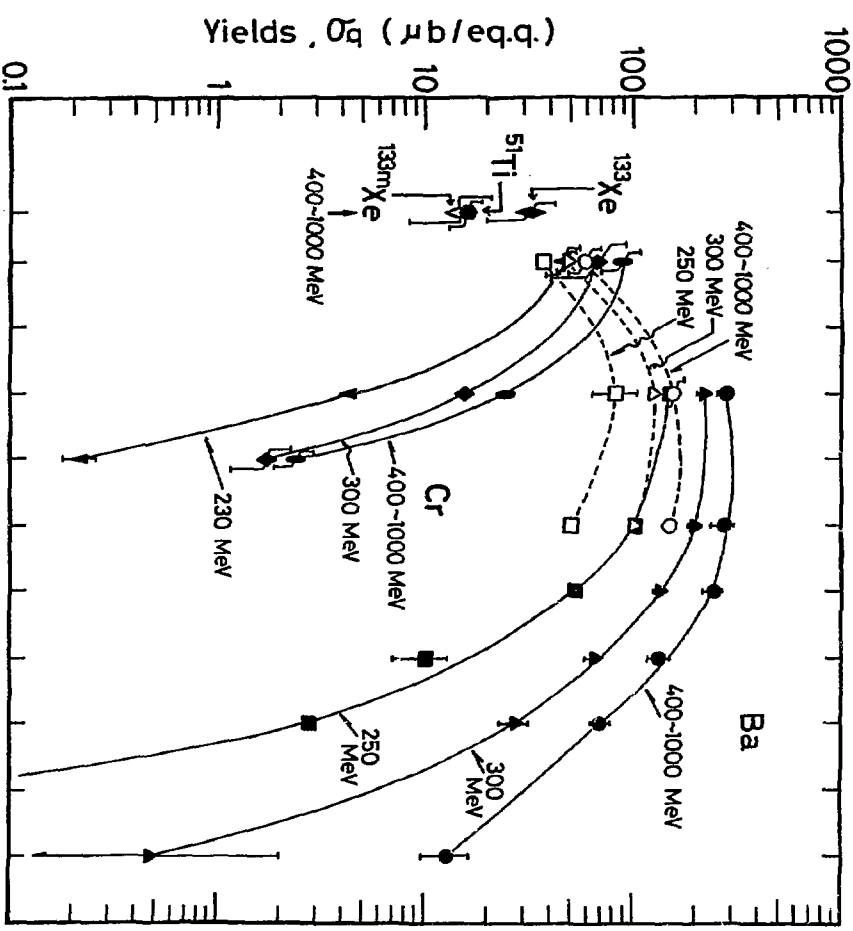
Yields , σq (μb/eq.q.)
1000
100
10
1
0.1
Number of emitted neutrons, x
0 1 2 3 4 5 6 7 8 9
133Xe
51Ti
133mXe
400-1000 MeV
400-1000 MeV
300 MeV
250 MeV
Ba
400-1000 MeV
300 MeV
250 MeV
Cr
400-1000 MeV
300 MeV
230 MeV

Fig. 3

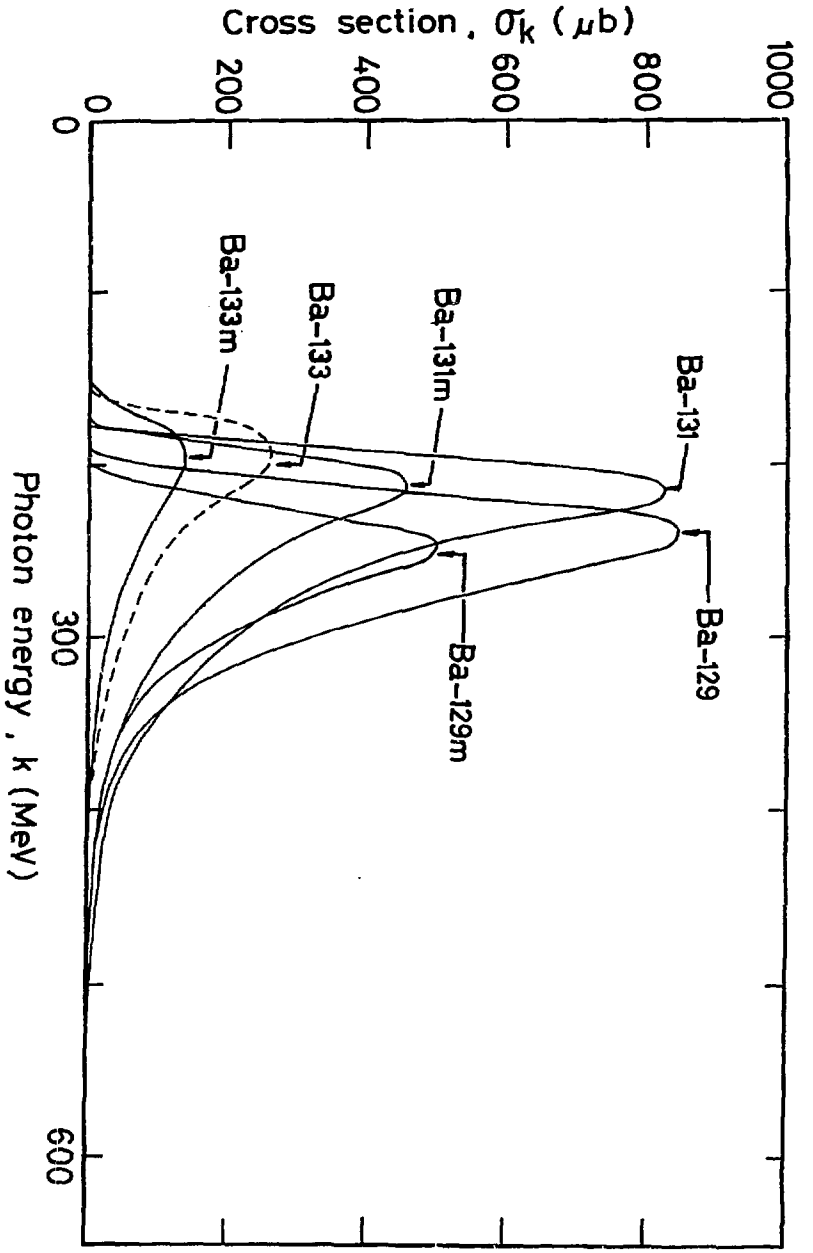
Cross section, σ_k (μb)
0
200
400
600
800
1000
Photon energy, k (MeV)
0
300
600
Ba-133m
Ba-133
Ba-131m
Ba-131
Ba-129
Ba-129m

Fig. 4(a)

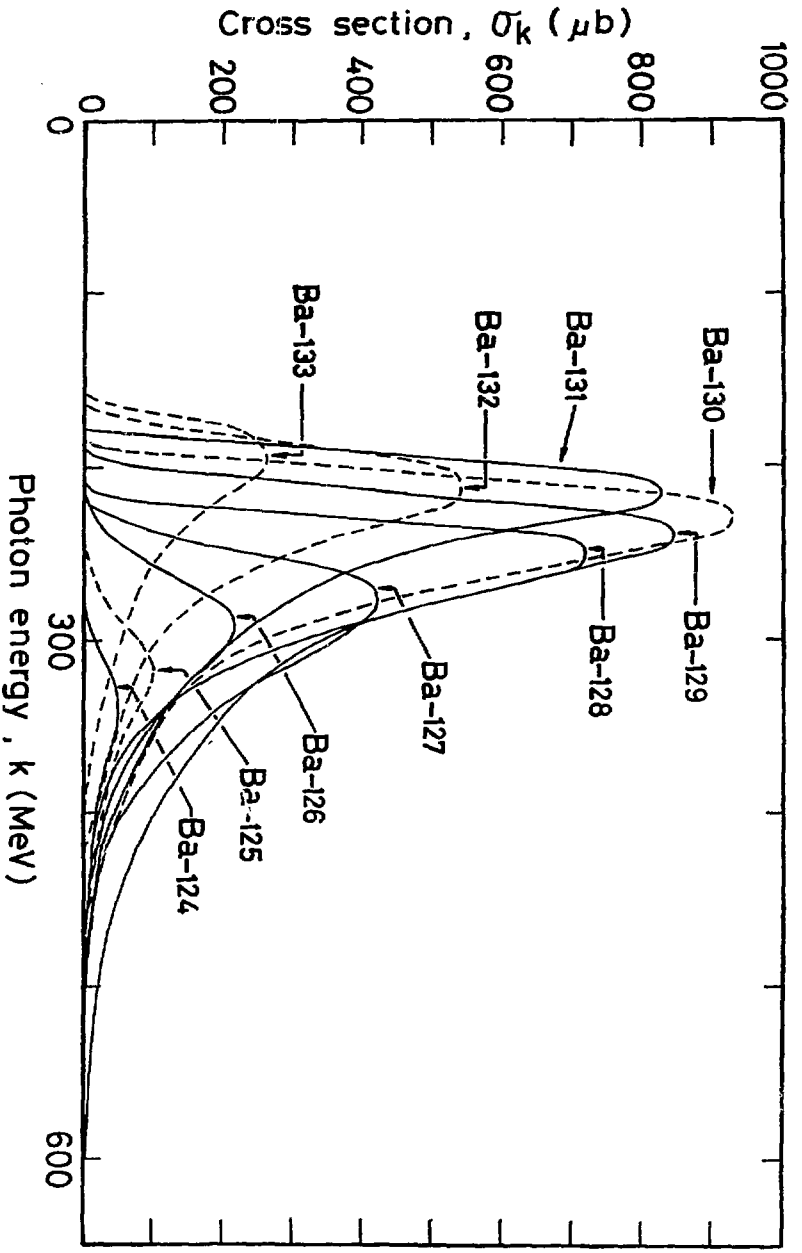
Cross section , σ_k (μb)
0
200
400
600
800
1000
Photon energy , k (MeV)
300
600
Ba-130
Ba-131
Ba-132
Ba-133
Ba-129
Ba-128
Ba-127
Ba-126
Ba-125
Ba-124

Fig. 4(b)

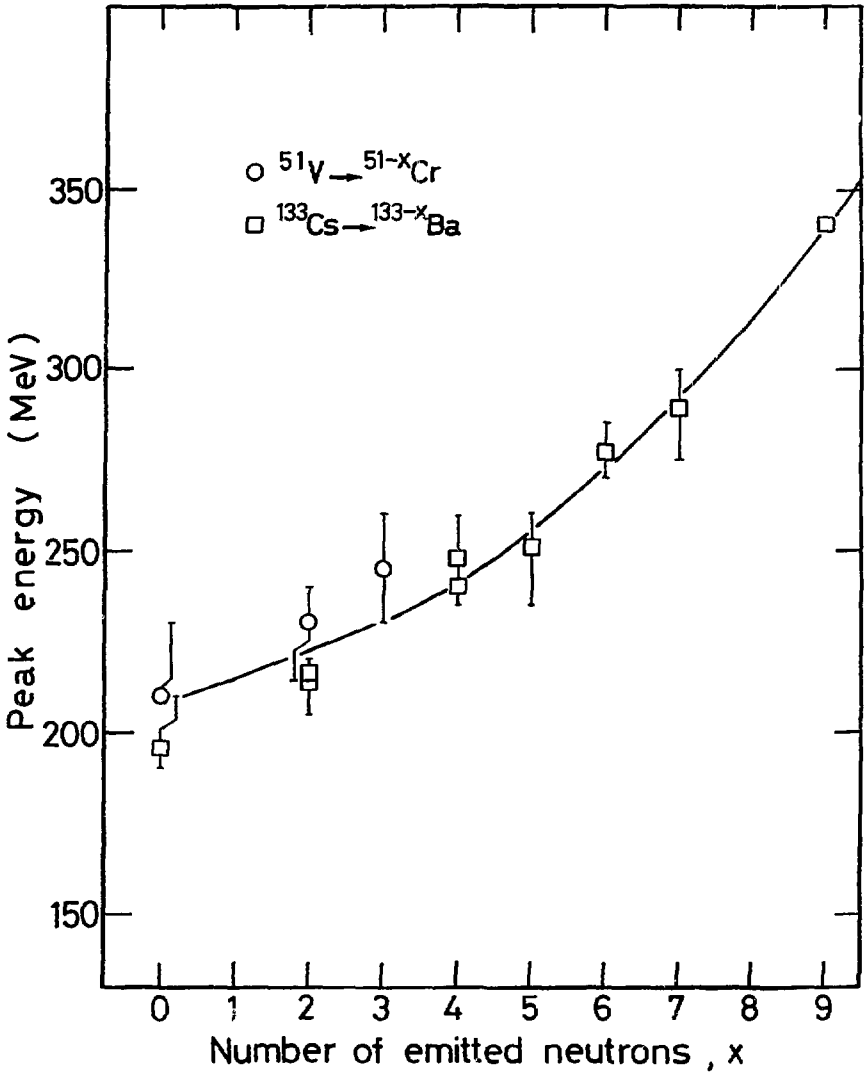
○ $^{51}V \rightarrow ^{51-x}Cr$
□ $^{133}Cs \rightarrow ^{133-x}Ba$
Peak energy (MeV)
350
300
250
200
150
0
1
2
3
4
5
6
7
8
9
Number of emitted neutrons , x

Fig. 5

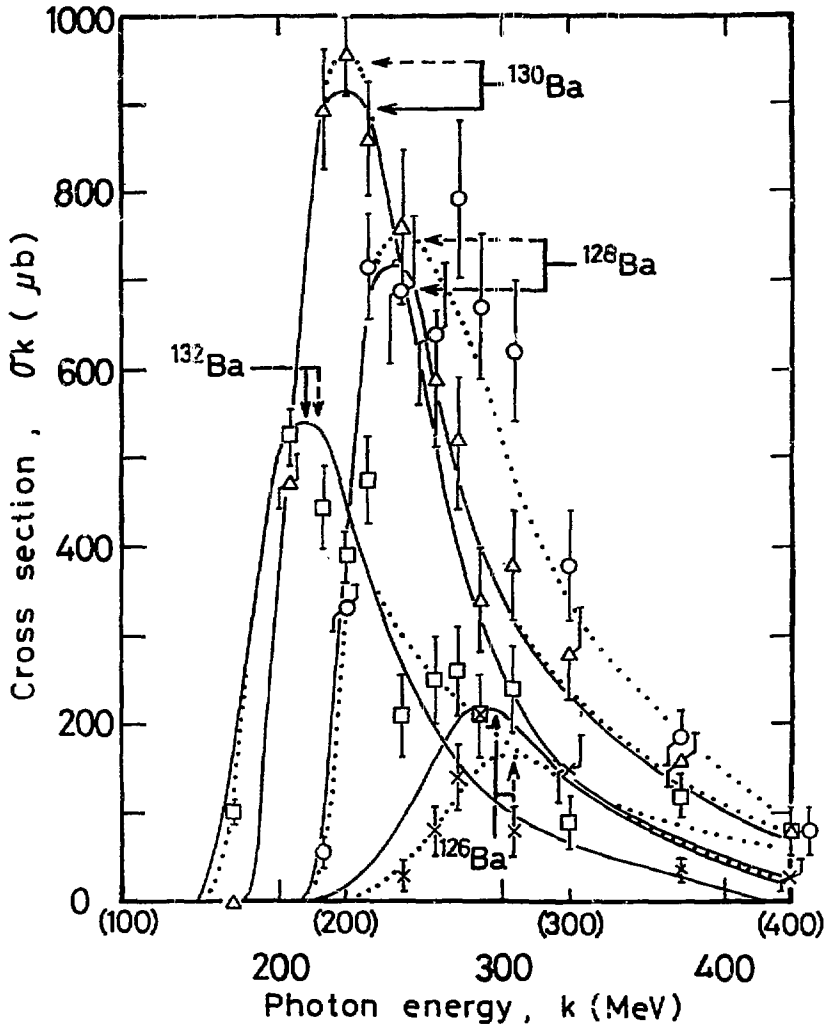
1000
800
600
400
200
0
Cross section , σk (μb)
130Ba
128Ba
132Ba
126Ba
(100)
(200)
(300)
(400)
200
300
400
Photon energy , k (MeV)

Fig. 6(a)

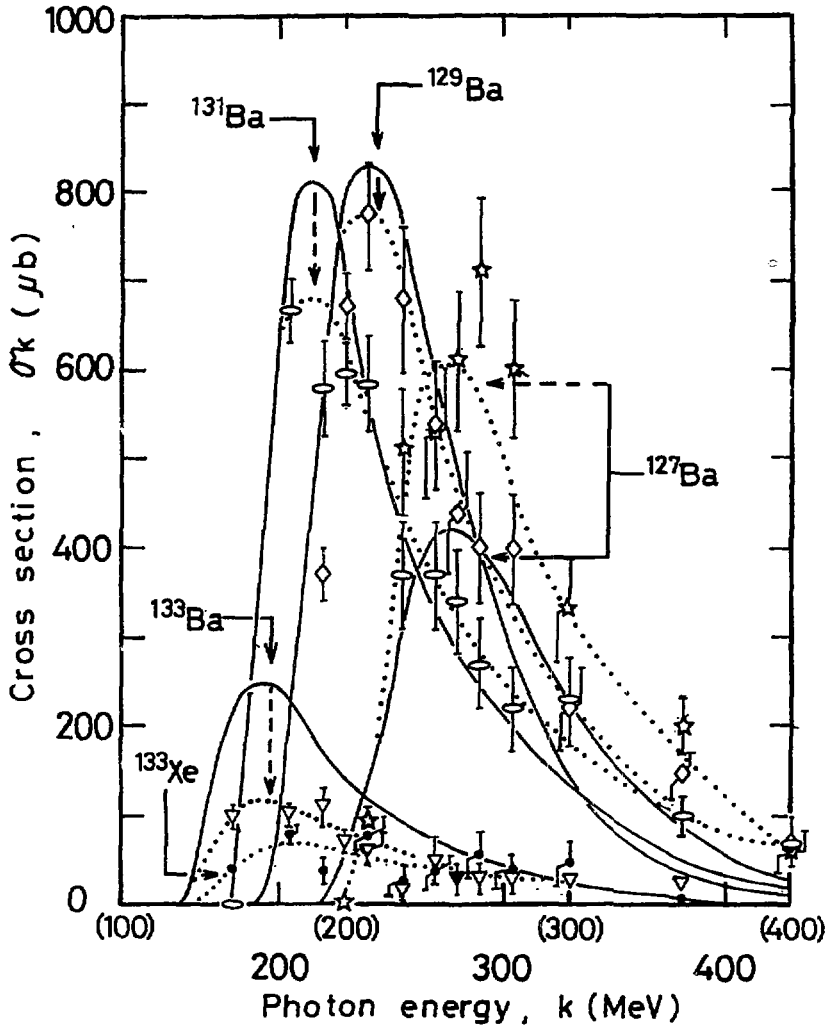
1000
800
600
400
200
0
Cross section, σk (μb)
131Ba
129Ba
127Ba
133Ba
133Xe
(100)
(200)
(300)
(400)
200
300
400
Photon energy, k (MeV)

Fig. 6(b)

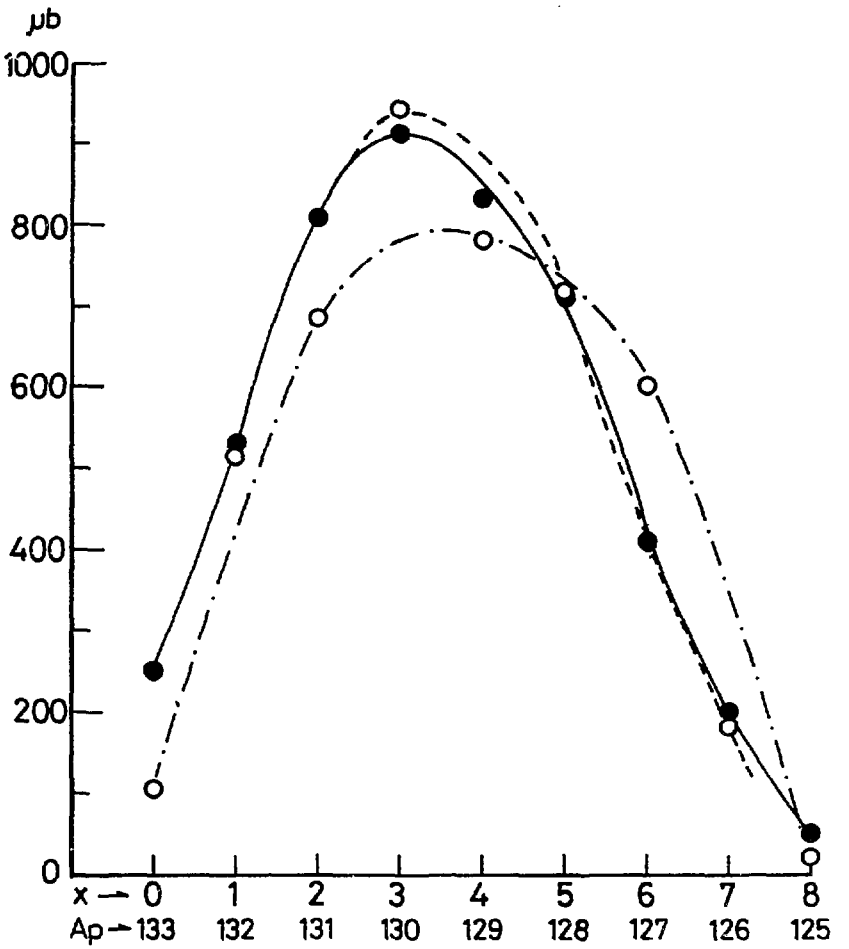
μb
1000
800
600
400
200
0
x → 0 1 2 3 4 5 6 7 8
Ap → 133 132 131 130 129 128 127 126 125

Fig. 7

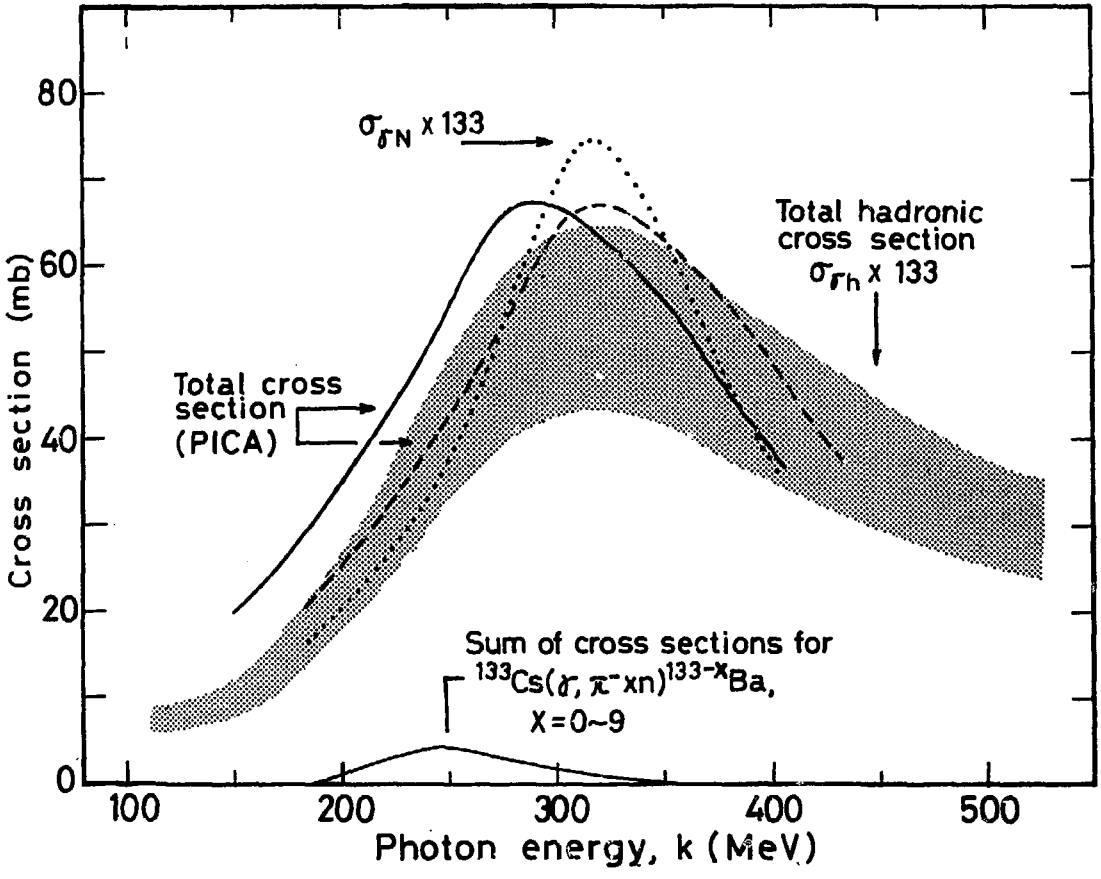
80
60
40
20
0
Cross section (mb)
100
200
300
400
500
Photon energy, k (MeV)
$\sigma_{\gamma N}$ x 133
Total hadronic
cross section
$\sigma_{\gamma h}$ x 133
Total cross
section
(PICA)
Sum of cross sections for
$^{133}Cs(\gamma, \pi^- xn)^{133-x}Ba$,
X=0~9

Fig. 8